Establishment of a Congenic Strain for the Oyster mushroom reveals the Structure and Evolution of Mating-Type Loci

Yi-Yun Lee[1], Guillermo Vidal-Diez de Ulzurrun[1], Rebecca J. Tay[2], and Yen-Ping Hsueh[1,2*]

[1] Department of Complex Biological Interactions, Max Planck Institute for Biology, Tübingen, Germany

[2] Institute of Molecular Biology, Academia Sinica, Nangang, Taipei, Taiwan

[*] Corresponding author

Email: yphsueh@tuebingen.mpg.de

Key words: oyster mushrooms, *Pleurotus ostreatus*, congenic strain, mating-type loci

Abstract

Pleurotus ostreatus, a widely cultivated edible oyster mushroom, is an ecologically versatile species with applications in biotechnology, agriculture, and food production. It functions as a decomposer and in nutrient-limited conditions it enhances its survival by using a potent toxin to prey on nematodes. Its adaptability is further regulated by sexual reproduction, which follows a tetrapolar mating system governed by two unlinked, multiallelic loci, *matA* and *matB*. The two mating-compatible monokaryotic strains PC9 and PC15, derived from the parental dikaryon strain N001, exhibit significant physiological differences. PC9 grows robustly in laboratory conditions, whereas PC15 grows more slowly, making PC9 the preferred strain for research. To advance *P. ostreatus* as a genetic model, we characterized the mating-type (*MAT*) loci of both monokaryon strains and developed a congenic strain. We analyzed the *MAT* loci in multiple *P. ostreatus* strains, and identified 11 A and 12 B alleles among twelve haplotypes, confirming their multiallelic nature. Using genetic backcrosses, we introgressed the *matA* and *matB* loci from PC15 into the PC9 genetic background to generate the congenic strain PC9.15. After sequencing and assembling a high-quality and contiguous genome for PC9.15, we confirmed that the genomes of PC9.15 and PC9 are 99% similar, with the only major difference placed at the *matA* and *matB* loci.

Author Summary

Mushrooms are not just decomposers—they can also be predators. The oyster mushroom *Pleurotus ostreatus* is an ecologically adaptable species that thrives by breaking down plant material and preying on nematodes using a potent toxin that triggers rapid paralysis of nematode prey. In addition to its ability to switch from saprophyte to predator, another feature contributing to the ecological success of *Pleurotus* is its reproductive strategy. *P. ostreatus* reproduces sexually through a tetrapolar mating-type system, governed by two unlinked mating loci, *matA* and *matB*. These loci determine mating compatibility and contribute to genetic diversity, yet their precise structure and allelic diversity remain unclear. In this study, we characterized the *matA* and *matB* loci in *P. ostreatus* strains PC9 and PC15 and analyzed *MAT* loci across multiple strains, confirming their multiallelic nature. To enhance *P. ostreatus* as a genetic model, we developed the congenic strain PC9.15 by introgressing *MAT* alleles from PC15 into the PC9 genetic background through genetic backcrosses. Genome sequencing confirmed that PC9.15 closely matches the genome of PC9, except at the *MAT* loci. This study expands our understanding of mating-type diversity in *P. ostreatus*, introduces PC9.15 as a valuable tool for genetic studies and controlled crosses, and facilitates the development of *P. ostreatus* as a model system for fungal biology.

56 # Introduction

57 The edible oyster mushroom *P. ostreatus* is a fascinating organism with significant
58 ecological and industrial importance. It is one of the most widely cultivated edible
59 mushrooms worldwide and an ecologically versatile species, thriving as a decomposer
60 in forests on decaying wood and forest litter (1, 2). Nutrient-limited environments can
61 trigger a shift in *P. ostreatus* toward carnivory to supplement its nutrient intake. *P.*
62 *ostreatus* preys on nematodes by producing a potent toxin, 3-octanone, which is
63 concentrated and stored inside specialized structures called toxocysts. Upon release,
64 this toxin rapidly paralyzes nematodes within minutes (3-5), allowing the fungus to
65 consume the immobilized prey. This ability to exploit multiple nutrient sources using
66 two different lifestyles contributes to *Pleurotus*'s adaptability and ecological success.

67 Like many fungi, *P. ostreatus* relies on sexual reproduction to maintain genetic
68 diversity and adaptability (2). In fungi, sexual reproduction is regulated by mating-type
69 loci (*MAT*), which determine compatibility and control genetic exchange between
70 individuals (6). Fungal mating systems are classified into heterothallism, where
71 individuals require a genetically compatible partner, or homothallism, which is
72 characterized by self-fertilization (7). The *MAT* loci of fungi have evolved into two
73 different organization paradigms: the bipolar and tetrapolar systems (8). In bipolar
74 mating systems, the homeodomain (*HD*) and pheromone/pheromone receptor (*P*/*R*)

75 genes are linked at a single *MAT* locus which determines sexual compatibility, requiring
76 two isolates to carry opposite alleles at this locus for successful mating (6). Conversely,
77 tetrapolar mating systems involve two unlinked *MAT* loci: the *HD* locus, encoding two
78 homeodomain-type transcription factors, and the *P*/*R* locus, which contains tightly
79 linked mating pheromones and pheromone receptors; mating in tetrapolar systems
80 requires distinct alleles at both loci for compatibility (6). Among Basidiomycetes, the
81 majority of species retain this ancestral tetrapolar mating system. However, in certain
82 lineages such as *Cryptococcus neoformans* and *Ustilago hordei*, the two loci have fused,
83 resulting in a derived bipolar mating system (9, 10). *P. ostreatus* follows a heterothallic
84 bifactorial tetrapolar mating system, where sexual compatibility is determined by two
85 unlinked, multiallelic loci, *matA* and *matB* (11, 12). Analyses of 17 *P. ostreatus* strains
86 have revealed at least ten distinct *matA* alleles and eight *matB* alleles, confirming the
87 extensive allelic diversity at both loci (13). Two widely used monokaryotic strains, PC9
88 and PC15, have been derived from the parental dikaryotic strain N001 through a process
89 that isolates distinct haploid nuclei called dedikaryotization (14). PC9 carries the
90 mating type *A2B1*, while PC15 harbors *A1B2* (14). Although the mating-type loci of *P.*
91 *ostreatus* have been described previously (13), their detailed structural organization and
92 allelic diversity remain incompletely characterized. A deeper understanding of these
93 loci is crucial for elucidating the molecular basis of mating compatibility and

94 identifying potential structural variations between strains.

95 Congenic strains serve as invaluable tools for genetic studies, retaining the genetic
96 identity of a parental strain while incorporating a specific region of interest. Such strains
97 enable precise investigations into complex genetic pathways and have been used to
98 study the function of mating-type loci in sexual and unisexual reproduction, virulence,
99 uniparental mitochondrial inheritance, and enable efficient genetic mapping and bulked
100 segregant analysis (BSA) in various fungal models (15-17). Despite their broad utility,
101 congenic strains are not available in *P. ostreatus*, limiting efficient genetic analyses and
102 manipulation in this species. A clear need for congenic strains in *P. ostreatus* emerges
103 from a genomic comparison between two commonly used laboratory strains, PC9 and
104 PC15. The PC9 and PC15 genomes align with approximately 97% identity over 94%
105 of the genome, with the remaining 6% showing no alignment (18). This high level of
106 genetic variation likely contributes to two strains' differing physiological characteristics:
107 PC9 grows at least twice as fast as PC15 in laboratory conditions, highlighting the
108 significant impact of their genetic differences and making PC9 the preferred laboratory
109 reference strain (18).

110 Here, we report the characterization of the *MAT* loci and the development of a
111 congenic strain of *P. ostreatus*, PC9.15, through ten genetic backcrosses. We sequenced
112 and assembled the PC9.15 genome using a long-read (Nanopore) sequencing, enabling

113 comparison of the *MAT* loci and their flanking regions between PC9 and PC9.15. We
114 further compared the *MAT* loci among multiple *P. ostreatus* genomes and revealed its
115 multiallelic structure. From twelve haplotypes analyzed, we identified 11 distinct alleles
116 at *matA* and 12 at *matB*, highlighting the remarkable genetic diversity of the *MAT* loci
117 in the *P. ostreatus* population. The development of the congenic strain, PC9.15, in the
118 genetic background of the model strain PC9, enhances the genetic toolkit for *P.*
119 *ostreatus*, offering a powerful genetic tool and resource to advance research in
120 mushroom biology.
121

122 # Results

123 ## Characterization of the mating-type loci in *P. ostreatus* strains

124 ## PC9 and PC15

125 High-quality genome assemblies of *P. ostreatus* strains PC9 and PC15 are available
126 (18-21), yet the mating-type loci remain incompletely characterized. In basidiomycetes,
127 the *matA* locus is typically flanked by the highly conserved mitochondrial intermediate
128 peptidase (*MIP*) and *β*-flanking (*βFG*) genes (22). Using these conserved flanking
129 genes, we identified and characterized the boundaries of the *P. ostreatus matA* locus.
130 The locus spans ~5kb in PC9 and ~10kb in PC15, both located on chromosome 2 (Fig
131 1A). The *matA* locus encodes two homeodomain (*HD*) genes, *HD1* and *HD2*, which
132 can form heterodimers with compatible HD proteins from the opposite mating partner,
133 enabling intracellular recognition of sexual compatibility after mating (23). Notably,
134 PC9 carries two HD genes (*HD1.1* and *HD2.1*) transcribed in opposite directions,
135 whereas, PC15 harbors four *HD* genes (*HD1.2*, *HD1.3*, *HD2.2*, and *HD2.3*) in the *HD*
136 locus (Fig 1A), suggesting a gene duplication event in PC15. A previous study reported
137 only a single *HD2* gene in the PC15 *matA* locus (13); however, examination of the JGI
138 genome assembly confirmed the presence of two *HD2* genes, consistent with the
139 complete gene content observed in our analysis. To assess allelic divergence, we aligned
140 the protein sequences of HD1 and HD2 from both strains. While all HD proteins share

141 conserved homeodomain motifs, we still observed distinct sequence variations among
142 HD1 and HD2 protein (S1A and B Fig), supporting the conclusion that PC9 and PC15
143 possess genetically distinct and mating-compatible *matA* alleles.

144 In both PC9 and PC15, the *matB* locus is located on chromosome 9, spanning ~54
145 kb and ~40 kb, respectively. The locus contains mating pheromone precursor (*PHB*)
146 and pheromone receptor (*STE3*) genes, which are involved in premating recognition (6).
147 Unlike the conserved flanking regions of *matA*, the *matB* locus is bordered by more
148 variable, species-specific genes (22). In both strains, *matB* is flanked by a general
149 substrate transporter (*MFS*) and a prenyltransferase (*UbiA*), providing genomic
150 boundaries for this locus. To identify the mating-type genes within *matB*, we searched
151 for conserved Pfam domains corresponding to *STE3* (Pfam: PF02076) and *PHB* (Pfam:
152 PF08015) domains. In total, four *STE3* genes (*STE3.1* to *STE3.4*) and five *PHB* genes
153 (*PHB1* to *PHB5*) were identified in PC9, and five *STE3* genes (*STE3.7* to *STE3.11*) and
154 six *PHB* genes (*PHB6* to *PHB11*) were identified in PC15 (S1 Table). Four additional
155 genes encoding Ste3 proteins, *STE3.5*, *STE3.6*, *STE3.12*, and *STE3.13*, that share high
156 sequence identity (> 96%) were found flanking the *matB* locus, suggesting that they are
157 not mating-type-specific (S2 Table). Alignment of all nine *STE3* receptors encoded in
158 the *matB* locus revealed notable variation in the C-terminal regions (S1C Fig),
159 consistent with their roles in mating signal recognition and allelic specificity. We further

160 identified genes that encode mating pheromone precursors (*PHB*) within the *matB* locus.
161 Across both alleles, we identified 11 *PHB* genes encoding peptides of 51 to 72 amino
162 acids in length with a canonical C-terminal CAAX motif (C = cysteine, A = aliphatic
163 residue, X = any residue) characteristic of mating pheromones (24). Protein sequence
164 alignment confirmed conservation of this motif among all *P. ostreatus* Phb peptides
165 (S1E Fig).

166 To explore the evolutionary divergence of mating-type genes across
167 basidiomycetes, we constructed maximum-likelihood phylogenetic trees of HD and
168 Ste3 protein from *P. ostreatus* and the model mushroom *Schizophyllum commune* (Fig
169 1B). Phylogenetic analysis of HD proteins revealed two distinct, well-supported clades
170 corresponding to HD1 and HD2 (bootstrap support = 100%). Within each clade,
171 sequences clustered by species, forming subgroups indicative of taxon-specific
172 diversification (Fig 1B). The clear separation between HD1 and HD2, along with their
173 internal species-level groupings, suggests long-term evolutionary maintenance and
174 potential functional specialization of these mating-type genes. In contrast, Ste3 proteins
175 grouped first by allele type and then further separated by species (Fig 1B). Within these,
176 Ste3.2 and Ste3.3 were highly similar to Ste3.8 and Ste3.9, respectively (S1D Fig). By
177 contrast, the protein sequences of Ste3.1 versus Ste3.7 and Ste3.4 versus Ste3.11 are
178 considerably more divergent, further supporting their roles as distinct mating-type

179 pheromone receptors (S1D Fig).

180

181 Multiallelic mating-type loci in *P. ostreatus*

182 In tetrapolar fungi, mating-type loci are often multiallelic rather than biallelic, resulting
183 in the presence of hundreds or even thousands of mating-types, as seen in *C. cinereus*
184 and *S. commune*, which have over 12,000 and 20,000 mating types, respectively (25).
185 *P. ostreatus* also follows a multiallelic tetrapolar mating system, though the exact
186 structure and diversity of its mating-type alleles remain poorly characterized. To
187 investigate its multiallelism, we compared the *matA* and *matB* loci across several *P.*
188 *ostreatus* genomes (Table 1). Our dataset comprised two monokaryotic strains, SS5 and
189 SS14, derived from strain TWF713, as well as additional publicly available *P. ostreatus*
190 genomes retrieved from NCBI and JGI databases. These include monokaryotic strains
191 CCMSSC00389 (389) (26), CCMSSC03989 (3989) (27), two haplotypes of the
192 dikaryotic strain gfPleOstr1.1 (gf and gfalt) (28), and the dikaryotic strains DSM11191
193 (DSM) and 595 (29). We then examined the *matA* and *matB* regions across all strains,
194 focusing on their organization, gene content, and allelic variation to better understand
195 the molecular basis of multiallelism in *P. ostreatus*.

196 Comparison of *HD* genes across ten *P. ostreatus* genomes revealed 17 *HD1* and
197 12 *HD2* alleles within these *matA* loci (Fig 2A and S3 Table). While at least 12 distinct

198 *matA* alleles have been reported previously (11), their structural organization and
199 sequence-level variation were not described. To avoid potential overlap with existing
200 allele designations, we named the characterized alleles in this study from A21-A29.
201 However, we cannot rule out the possibility that some of these may be identical in
202 sequence or in mating type to previously reported alleles. SS14 shares an identical *matA*
203 allele with PC9 (allele A2), while nine novel *matA* alleles were identified among the
204 remaining haplotypes (Fig 2A). Six haplotypes contained a single *HD1*/*HD2* gene pair
205 (Fig 2A), although duplication of *HD1* was observed in SS5 (*A21*), 389 (*A22*), and 595
206 (*A26*). Notably, SS5 (*A21*) carries three *HD1* genes, a configuration similar to that
207 recently reported for *P. ostreatus* strain PC80, derived from an artificially cultivated
208 strain HeiKang 650 (30). The gfalt haplotype (*A29*) exhibited duplication of both *HD1*
209 and *HD2*, consistent with our previous observations in PC15. Moreover, the *matA* locus
210 of gfalt (A29) expanded to 73 kb—substantially larger than the 6 kb locus in PC9—and
211 contained an insertion of five genes, including four hypothetical proteins and one
212 transposase (Fig 2A). Given the sequence variation and gene duplications we had
213 observed, we performed phylogenetic analysis to assess the divergence of HD1 and
214 HD2 proteins across strains. This analysis revealed two distinct clusters for HD1
215 (HD1.1 to HD1.17) and HD2 (HD2.1 to HD2.13), confirming the divergence of these
216 gene families (Fig 2B).

217 At the *matB* locus, we identified ten new alleles (B21-B30) that are absent in either
218 PC9 or PC15, with locus sizes ranging from 45 kb to 150 kb (Fig 2A). The locus is
219 flanked by *MFS* and *UbiA* genes, and most alleles contain three to five *STE3* and four
220 to six *PHB* genes. One to two *STE3*-like genes were also found immediately outside
221 the *UbiA* boundary in different strains; these receptors share high similarity and
222 therefore were considered non-mating-type-specific. The *matB* loci of SS5 (B21), SS14
223 (B22), and 595 (B28) were notably expanded—to 105 kb, 77 kb and 150 kb,
224 respectively—compared to the 54 kb locus in PC9. Several additional genes were
225 detected within these expanded regions, including an integrase, a retrotransposon Gag
226 protein, and hypothetical proteins, which are unlikely to be directly involved in mating
227 but may have contributed to the locus expansion. Phylogenetic analysis of Ste3 protein
228 sequences illustrates their diversity across *P. ostreatus* strains, aligning with the
229 multiallelic nature of the *matB* locus and with the locus's role in facilitating diverse
230 mating interactions (Fig 2B). In total, we identified distinct 12 *matB* distinct alleles
231 across strains containing 48 *STE3*-like pheromone receptor genes, confirming the
232 multiallelic configuration of both loci in *P. ostreatus*.

233 To test whether allelic variation affects mating compatibility, we performed
234 reciprocal crosses among SS5 (*A21B21*), SS14 (*A2B22*), PC9 (*A2B1*) and PC15 (*A1B2*).
235 SS5 is compatible with both PC9 and PC15, as evidenced by the presence of clamp

236 connections—hallmark structures of dikaryotic hyphae in basidiomycetes—and
237 successful fruiting body development (Fig 2C). The SS14 x PC9 cross produced neither
238 clamp connections nor fruiting bodies, as expected from their both harbor the *A2* allele
239 of the *matA* locus (Fig 2C). In contrast, the SS14 x PC15 cross yielded clamp
240 connections and fruiting bodies (Fig 2C). These results support that *P. ostreatus* follows
241 a tetrapolar mating system, in which successful mating requires compatibility at both
242 *matA* and *matB* loci.

243 **Table 1. *P. ostreatus* genomes used in the present study.**

Strain (haplotype)	Genome size	BUSCO (%)	Source	Citation
PC9	35.0 Mb	98.6% [S:97.3%, D:1.3%]	NCBI	(18)
PC15	34.3 Mb	99.3% [S:98.0%, D:1.2%]	NCBI	(19-21)
SS5	41.4 Mb	99.4% [S:95.9%, D:3.5%]	this study	this study
SS14	43.6 Mb	99.4% [S:91.2%, D:8.2%]	this study	this study
CCMSSC00389	35.1 Mb	98.8% [S:97.4%, D:1.4%]	NCBI	(26)
CCMSSC03989	34.4 Mb	98.9% [S:97.8%, D:1.1%]	NCBI	(27)
gfPleOstr1.1	40.6 Mb	99.4% [S:98.2%, D:1.2%]	NCBI	(28)
gfPleOstr1.1 alternate haplotype	40.8 Mb	99.1% [S:97.4%, D:1.7%]	NCBI	(28)
DSM11191	65.9 Mb	99.5% [S:6.6%, D:92.9%]	JGI	
595	79.7 Mb	99.7% [S:25.7%, D:74.0%]	NCBI	(29)

244

245

246

247

248 **Construction of the congenic strain PC9.15 via genetic**
249 **backcrossing**

250 PC9 and PC15 are monokaryotic strains derived from the dikaryotic strain N001, but
251 only ~94% of their genomes are aligned with high similarity (~97%). This high genetic
252 diversity likely contributes to the significant growth differences observed between the
253 two strains. Given the robust growth and well-annotated genome of PC9, we selected
254 the PC9 genetic background for introgression of the PC15 mating-type loci to generate
255 a congenic strain (Fig 3A). To construct a congenic strain with PC9 background, we
256 first crossed PC9 and PC15 and isolated meiotic progeny by dissecting individual
257 basidiospores. Randomly selected progeny carrying the *A1B2* mating type as
258 determined by PCR was then backcrossed with PC9 (*A2B1*). After nine additional
259 rounds of backcrossing, we obtained a congenic strain that we designated PC9.15,
260 which carries the *A1B2* mating-type loci from PC15 (Fig 3B and S2A Fig). We found
261 that PC9.15 exhibited growth behavior comparable to PC9 on nutrient-rich medium
262 (YMG) and readily formed fruiting bodies when crossed with PC9 (Fig 3A and 3C).
263 Overall, phenotypic characterization of PC9.15 showed that it retains growth and
264 reproductive traits of PC9 while carrying the *A1B2* mating-type loci from PC15.

265

266 **High-quality genome assembly and analysis of the congenic**

267 **strain PC9.15**

268 To confirm the genome similarity of PC9.15 to PC9 and to characterize its
269 chromosomal architecture, we generated a high-quality, near-chromosome-level
270 genome assembly of the *P. ostreatus* congenic strain PC9.15. Using Nanopore
271 sequencing, we achieved 128x coverage and assembled a contiguous genome of ~35.3
272 Mb (Table 2), comparable to the genome sizes of PC9 (35.0 Mb) and PC15 (34.3 Mb)
273 (18-21). The PC9.15 genome is distributed across 14 scaffolds, ranging from 38.7 kb
274 to 5.36 Mb, including one scaffold representing the mitochondrial genome. Among the
275 11 main scaffolds analyzed, nine exhibit telomere-to-telomere assembly, one possesses
276 telomeric repeats at a single end, and one lacks telomeric sequences. Although *P.*
277 *ostreatus* is known to contain 11 chromosomes (14), our assembly of PC9.15 includes
278 13 scaffolds. The two additional scaffolds, representing only 1.4% of the total genome
279 size, likely representing unresolved gaps or unplaced regions, such as centromeric or
280 telomeric sequences. For example, scaffold 12 (468,928 bp) contains telomeric repeats
281 and may correspond to a terminal chromosome region, while scaffold 13 (38,780 bp)
282 shows high coverage depth but without gene density, a characteristic associated with
283 centromeres (31), suggesting it may represent a misplaced centromeric fragment.
284 Collectively, these results indicate that the PC9.15 genome assembly reaches near-
285 chromosome-level resolution, with 11 chromosome-like scaffolds.

286 To assess genome completeness and structural features of the PC9.15 assembly,
287 we analyzed gene density, sequence coverage, and BUSCO scores. Gene density is
288 consistent across 11 scaffolds, averaging approximately 41 genes per 100 kb, with an
289 average sequencing depth of 71.8 reads per 10 kb (Fig 4A). Coverage is generally
290 uniform across chromosomes, with localized increases on chromosomes 2 and 6 (Fig
291 4A), possibly due to repetitive sequences, such as transposable elements (TEs).
292 Assembly completeness, assessed using the basidiomycota_odb10 database (32),
293 yielded a BUSCO score of 99.4%, comparable to that of PC9 (98.6%) and PC15 (99.3%)
294 (18), confirming the high quality of the PC9.15 assembly. Overall, these results confirm
295 that the PC9.15 genome is well-assembled, complete, and suitable for further genomics
296 analysis.

297 To evaluate genomic similarity and structural variation, we compared the PC9.15
298 genome to its parental strains, PC9 and PC15. Annotation of the PC9.15 genome using
299 *funannotate* (v1.8.14) (33) identified 14,118 genes (S5 Table), higher than in PC9
300 (11,875 genes) (18) or PC15 (12,330 genes) (19-21). To control for annotation
301 inconsistencies arising from version differences, we re-annotated the PC9 genome
302 using the same version of *funannotate* (v1.8.14), which yielded 12,003 genes. Therefore,
303 the higher gene count observed in PC9.15 likely reflects a combination of improved
304 assembly contiguity and enhanced performance of newer *funannotate* versions. To

305 assess genome-wide similarity, we used D-Genies to generate dot-plot alignments
306 between PC9.15 and its parental strains, PC9 and PC15 (34). The comparison revealed
307 ~99.47% sequence similarity between PC9 and PC9.15 genomes (defined by >75%
308 identity) (Fig 4B), whereas PC9.15 and PC15 shared ~56.31% similarity under the same
309 threshold. This demonstrates that PC9.15 is genetically closer to PC9, consistent with
310 its congenic background. Comparative analysis revealed several chromosomal
311 rearrangements in PC9.15 relative to PC9. Circos plot alignment showed that a segment
312 from PC9 chromosome 4 had been translocated to PC9.15 chromosome 2, and a region
313 from PC9 chromosome 7 translocated to and became inverted on PC9.15 chromosome
314 4 (Fig 4C). Additionally, we observed a unique region (segment A) on chromosome 4
315 of PC9.15 that did not align with the PC9 genome (Fig 4C), but partially matched
316 chromosome 4 of PC15 (Fig 4D), indicating that this region retains PC15-derived
317 sequence. The persistence of this segment may reflect suppressed recombination,
318 potentially caused by repetitive sequences, structural rearrangements, or local
319 chromosomal features that reduce crossover frequency, as observed in analogous
320 recombination-suppressed regions (35).
321
322
323

324 **Table 2. Genomic features of three *P. ostreatus* genome assemblies: PC9, PC9.15,**

325 **and PC15. nt, nucleotides.**

General features	PC9	PC9.15	PC15
Total nt	35,032,978	35,378,061	34,342,730
Number of chromosome-like scaffolds	11	11	11
N50 scaffold size, nt	3,500,734	3,339,398	3,270,165
N90 scaffold size, nt	2,134,864	1,697,083	1,880,400
Scaffold max. nt	4,859,873	5,366,244	4,830,258
Scaffold min. nt	9,086	38,780	280,724
Number of scaffolds	17	14	13
N50 contig size, nt	3,500,734	3,339,398	3,270,165
N90 contig size, nt	2,134,864	1,697,083	1,571,664
GC content, %	50.79	50.90	50.95
Genes	11,875	14,118	12,330
BUSCO completeness v6.0.0 (basidiomycota_odb10), %	98.6	99.4	99.3

326

327 Analysis of mating-type loci in the congenic strain PC9.15

328 To confirm the mating-type configuration of the congenic strain PC9.15, we analyzed

329 the structure of its *matA* and *matB* loci and compared them to those of PC9 and PC15.

330 As in parental strains, the *matA* and *matB* loci of PC9.15 are located on chromosome 2

331 and 9, respectively. The *matA* locus contains four *HD* genes (*HD1.2*, *HD1.3*, *HD2.2*,

332 and *HD2.3*), and the *matB* locus includes five *STE3* genes (*STE3.7* to *STE3.11*) and six

333 pheromone precursor genes (*PHB6* to *PHB11*), identical to PC15 (Fig 5A and 5B).

334 These results confirm that PC9.15 carries the *A1B2* mating-type loci inherited from
335 PC15.

336 To further identify the recombination sites around the mating-type loci, we
337 expanded the sequence alignment to ~3 Mb for the *matA* locus and ~600 kb for the
338 *matB* locus (Fig 5C and 5D). PC9.15 retained segments of the PC15 genomic
339 background near both loci, with approximately 1.13 Mb around *matA* and 300 kb
340 around *matB*. These retained regions suggest suppression of recombination during
341 backcrossing in flanking regions of the two *mat* loci. Despite these regions of difference,
342 the remainder of the PC9.15 genome is largely derived from PC9. Together, these data
343 confirm the successful construction of a congenic strain that harbors the PC15 mating-
344 type loci (*A1B2*) within the PC9 genetic background.

345

346 Annotation of the PC9 mitochondrial genome in *P. ostreatus*

347 We annotated the PC9 mitochondrial genome, revealing a 65 kb circular molecule
348 similar to the mitochondrial genomes of *Neurospora crassa* (~65 kb) and
349 *Saccharomyces cerevisiae* (~79 kb). The mitochondrial genome of PC9 encodes 18
350 protein-coding genes, two rRNA genes (*rrnS* and *rrnL*), and 25 tRNA genes (Fig 6).
351 The protein-coding genes comprise three cytochrome c oxidase subunits (*COX1*, *COX2*,
352 *COX3*) from respiratory complex IV, seven NADH dehydrogenase subunits (*NAD1*,

353 *NAD2*, *NAD3*, *NAD4*, *NAD4L*, *NAD5*, *NAD6*) from complex I, three ATP synthase
354 subunits (*ATP6*, *ATP8*, *ATP9*) from complex V, as well as apocytochrome b (*COB*),
355 DNA-directed RNA polymerase (*RPO*), ribosomal protein (*RPS3*), and two DNA
356 polymerase (*DPO1* and *DPO2*). Given that PC9 and PC15 are descended from the
357 strain N001, we expected their mitochondrial genomes to be identical. Indeed, our
358 comparison showed 99.9% similarity between the mitochondrial genomes of PC9,
359 PC15, and PC9.15 (S3 Fig and S6 Table).

360 # Discussion

361 ## Diversity and genomic organization of mating-type loci in *P.*
362 ## *ostreatus*

363 In this study, we investigated the structure and diversity of *matA* and *matB* alleles in *P.*
364 *ostreatus*. Given the diversity of mating-type loci across basidiomycetes, we compared
365 our findings to other well-characterized systems. In *C. cinereus*, the *matB* locus is
366 organized into three distinct gene groups, each containing a single pheromone receptor
367 gene (*RCB*) and multiple pheromone genes (*PHB*) (36). Similarly, phylogenetic
368 analysis of Ste3 proteins in *P. ostreatus* revealed five distinct groups (Fig 2B). In most
369 *P. ostreatus* strains, *PHB* genes are located near *STE3* genes, and the number of *PHB*
370 genes is typically equal to or greater than the number of *STE3* genes. The frequent
371 proximity of *PHB* and *STE3* gene, and the higher number of *PHB* genes relative to
372 *STE3*, suggest a more flexible system of mating regulation. This organization may allow
373 *P. ostreatus* to fine-tune mating recognition through multiple pheromone-receptor
374 combinations. Unlike the tightly clustered arrangement seen in *C. cinereus*, this
375 dispersed structure likely reflects a different evolutionary path for generating mating-
376 type diversity. In *P. ostreatus*, genes encoding the MAP kinase signaling cascade (e.g.,
377 *STE20*, *STE11*, *STE12*) are dispersed across multiple chromosomes rather than residing
378 within a *MAT* locus as in *C. neoformans* (10). Instead, the *matB* includes several

379 reductases, transporters, and hypothetical proteins whose functions remain unclear but
380 may still play a role in mating.

381 The tetrapolar mating-type system, with multiallelic *matA* and *matB* loci, promotes
382 outcrossing in basidiomycetes (37). For example, in *C. cinerea*, over 200 alleles per
383 *MAT* locus yield a 99.5% outcrossing probability, whereas *Ustilago maydis*, with over
384 25 *b* alleles and only two *a* mating types, exhibits a lower outcrossing probability of
385 50% (38). The diversity of mating-type alleles in *P. ostreatus* likely enhances
386 outcrossing in natural populations. Our analysis identified 11 alleles at the *matA* locus
387 and 12 alleles at the *matB* locus across 12 *P. ostreatus* haplotypes, suggesting the
388 existence of at least 132 distinct mating types. These findings not only validate the
389 multiallelic structure of *P. ostreatus* mating-type loci but also provide a detailed
390 molecular characterization of allele diversity. Given this extensive allelic variation,
391 additional *matA* and *matB* alleles likely remain unidentified in natural populations.
392 Future studies on wild-isolated *P. ostreatus* strains will further enhance our
393 understanding of the diversity and complexity of these loci and provide deeper insights
394 into the evolution and regulation of the mating-type system in *P. ostreatus*.

395

396 Expansion and allelic diversity of *MAT* loci across strains

397 Across twelve *P. ostreatus* haplotypes, we identified 11 *matA* alleles and 12 *matB* alleles,

398 confirming extensive multiallelism at both *MAT* loci. We also observed significant
399 expansion in the physical size of these loci, including one expanded *matA* locus (73 kb
400 in the gfalt haplotype versus 6 kb in PC9) and three expanded *matB* loci (77-150 kb
401 versus 50 kb in PC9). The expanded regions contain additional genes, notably a
402 transposase, a intergrase/recombinase-like protein, and a retrotransposon Gag protein,
403 suggesting that transposable elements (TEs) and retrotransposon activity may has
404 contributed to the structural expansion. Similar TE-associated expansion of the *MAT*
405 locus has been reported in *Cryptococcus*, where accumulation of transposons within the
406 *MAT* region ha contributed to its expansion (39). Moreover, the transition from an
407 ancestral tetrapolar to a bipolar mating system in *Cryptococcus* involved fusion of the
408 previously unlinked *P/R* and *HD* loci via chromosomal translocations, resulting in an
409 expanded contiguous *MAT* locus (40). Together, these findings support the hypothesis
410 that TE insertions, together with integrase/recombinase activity, create a genomic
411 environment that promotes structural rearrangements while preserving mating-type
412 diversity in *P. ostreatus*.
413

414 Genomic rearrangement and recombination at the *MAT* loci

415 We identified recombination-suppressed regions surrounding both *MAT* loci, spanning
416 ~1.13 Mb around *matA* and ~300 kb around *matB*. The suppressed interval flanking

417 *matA* is significantly larger than the 10 kb *matA* locus itself, suggesting that additional,
418 yet unidentified, factors within this genomic region may contribute to reduced
419 recombination frequencies. Recombination suppression at *MAT* loci has been studied
420 in other fungi; for example, in *Neurospora*, recombination within the *MAT* region is
421 inhibited, preventing second-division segregation of mating type and thereby avoiding
422 the production of self-sterile ascospores (41). Similarly, a recent study in *Cryptococcus*
423 showed that recombination is suppressed not only at the *MAT* locus but also across large
424 centromere-linked domains enriched in repetitive elements and heterochromatin, and
425 that intercentromeric recombination can generate chromosomal translocations that
426 further increase suppression in these regions (42). Therefore, recombination
427 suppression at the *P. ostreatus MAT* loci may similarly result from centromere-linked
428 heterochromatin and repetitive DNA.

429 Comparative analysis revealed several chromosomal rearrangements in the
430 PC9.15 genome relative to PC9 and PC15. Chromosome translocations have been
431 previously documented between PC9 and PC15 (18), so it is not surprising that the
432 congenic strain also underwent large-scale rearrangements. For example, a portion of
433 PC9 chromosome 4 (C4) has translocated to chromosome 11 (C11) in PC15 (18), and
434 the same sequence (segment B) has translocated to chromosome 2 (C2) in PC9.15 (S4A
435 and C Fig). Initially, we hypothesized that segment B originated from the centromeric

436 region, which is often enriched in transposons and repetitive elements prone to
437 recombination errors, as observed in *C. neoformans* (10). However, further analysis
438 revealed that segment B is present on both chromosome 2 (C2) and chromosome 4 (C4)
439 in the PC9 genome, indicating that duplication events had occurred before the
440 translocation was observed (S4B and D Fig). These findings suggest that the
441 translocation of segment B likely resulted from recombination errors due to sequence
442 similarity between duplicated segments.

443 Collectively, this study provides a detailed characterization of the *P. ostreatus MAT*
444 loci in strains PC9 and PC15 and established PC9.15 as a congenic strain and a new
445 genetic resource for precise genetic studies. We identified a multiallelic mating-type
446 system with 11 *matA* and 12 *matB* alleles across twelve haplotypes. The PC9.15
447 congenic strain established here offers a versatile tool for probing the genetic and
448 evolutionary dynamics of mating-type loci and for conducting future functional studies
449 in this species.

450 # Materials and Methods

451 ## Strains and culture conditions

452 *Pleurotus ostreatus* strains PC9 and PC15 differentiated from dikaryotic strain N001
453 (11), were used as the starting parental strains for genetic crosses. Spores were collected
454 from a fruiting body of TWF713. Two monokaryon strains, SS5 and SS14, each
455 originating from a single basidiospore, were established in the laboratory for analysis.
456 Strains were maintained on yeast and malt extract with glucose (YMG) medium
457 solidified with 1.5% (w/v) agar and incubated at 25°C.

458 ## Crossing, fruiting conditions and isolation of meiotic progeny

459 To induce dikaryon formation, the mating-compatible monokaryotic strains PC9 and
460 PC15 were co-cultured on YMG agar medium for two weeks. Agar blocks from the
461 mating interface were then transferred into sterile bottles containing sawdust medium
462 (100 g of sawdust, 30 g wheat bran, tap water to 150 mL). These bottles were then
463 incubated at 25℃ in darkness for ten days. To induce fruiting body formation and obtain
464 F1 progeny, cultures were shifted to 15℃ under a 12 hr light/12 hr dark cycle. Fruiting
465 bodies appeared after approximately seven days and matured within 3-4 days. Spores
466 (F1 progeny) were harvested in Millipore water and micromanipulated using a
467 dissecting microscope, with each plate containing 18 basidiospores. To assess
468 reproductive performance, we recorded the number of germinated progeny per plate.

469 Individual progeny were cultured, and their mating types were determined by PCR
470 using mating-type-specific primers (S4 Table).

471 Congenic strain construction

472 PC9 was crossed with PC15, and single basidiospores were isolated. Three progeny
473 carrying the PC15 mating type were selected and backcrossed to PC9. This process was
474 repeated for a total of ten backcrosses to produce PC9.15, a congenic strain with mating
475 loci derived from PC15 in the PC9 genetic background.

476 Genome sequencing and assembly comparison

477 The congenic strain PC9.15 and the monokaryotic strains SS5, and SS14 were cultured
478 on YMG agar at 25°C for 7 days. Mycelia were then transferred to 50 mL of YMG
479 liquid medium and incubated at 25°C and shaken at 200 rpm for 4 days. Genomic DNA
480 was extracted using the cetyltrimethylammonium bromide (CTAB) method and
481 purified by extraction with chloroform and phenol-chloroform and precipitation with
482 isopropanol and ethanol, followed by an AMPure XP (Beckman Coulter) purification
483 step. Libraries were prepared using the genomic DNA by Ligation kit (SQK-LSK109),
484 and Nanopore long-read sequencing was performed using a FLO-MIN106 R9 flow cell
485 (Oxford Nanopore) for PC9.15 and a R10 version flow cell (Oxford Nanopore) for SS5
486 and SS14. This approach yielded ~0.6 M reads for PC9.15, with a mean length of 7,400
487 bp, resulting in ~128X genome coverage. For SS5 and SS14, sequencing produced

488 ~0.76 M and ~0.65M reads, with mean read lengths of 11,981 bp and 10,348 bp,
489 corresponding to ~202X and ~142X coverage, respectively. *De novo* assembly of
490 Nanopore long reads was performed using NECAT (43).
491 For comparison of the PC9, PC15, and PC9.15 genomes, we used the dnadiff program
492 from the MUMmer package (44), which computed sequence identity and generates
493 alignment statistics between them.

494 Genome annotation

495 Genome annotation for PC9.15, SS5, and SS14 was performed using *funannotate*
496 (v1.8.1) (33) and the pipeline described at
497 *https://funannotate.readthedocs.io/en/latest/index.html.* For PC9.15, we then used
498 *funannotate train* with RNA-seq data and masked genome to generate preliminary gene
499 models. RNA was extracted from the PC9.15 strain and sequenced on an Illumina
500 NextSeq 500 Mid Output 300 cycles using a paired-end 150 bp configuration (PE150).
501 For strains SS5, SS14, CCMSSC00389 (26), CCMSSC03989 (27), gfPleOstr1.1
502 (haplotypes gf and gfalt) (28), and 595 (29), gene prediction was performed directly
503 with *funannotate predict* after masking, without RNA-seq-based training. Functional
504 annotation was performed using the *funannotate remote* option, which incorporated
505 InterProScan and antiSMASH to identify InterPro domains and secondary metabolite
506 clusters, respectively. Finally, *funannotate annotate* was used to integrate functional

507 annotations, including Pfam domains, clusters of orthologous groups (COGs), and
508 EggNOG classifications. The full annotation of PC9.15 is provided in S5 Table.
509 The accession numbers of BioSample: SAMN05327826 (CCMSSC00389),
510 SAMN09434509 (CCMSSC03989), SAMN23459969 (595), SAMEA8562045
511 (gfPleOstr1.1), and SAMEA8562045 (gfPleOstr1 alternate haplotype).

512 Annotation of the PC9 mitochondrial genome

513 A putative large duplication in PC9 scaffold_14 was identified through self-alignment
514 of the sequence and is suspected to be an artifact resulting from the circular nature of
515 the mitochondrial DNA and overlapping regions in the assembled Nanopore reads. This
516 hypothesis was confirmed by aligning the contig with the mitochondria genome of *P.*
517 *ostreatus* P51 (45). The duplicated region was manually removed, resulting in an
518 assembled mitochondrial genome of PC9 that closely matched the size of the P51
519 mitochondria genome. Annotation was performed using MITOS2 (46).

520 Genome and mating-type loci comparison

521 General genome assembly statistics, including scaffold length and N50, were calculated
522 using the count_fasta_residues.pl script (*https://github.com/SchwarzEM/ems_perl/*
523 *blob/master/fasta/count_fasta_residues.pl*). Assembly completeness was assessed with
524 BUSCO v6.0.0 using the basidiomycota_odb10 database (32, 47). Repetitive elements
525 were identified using a custom repeat library generated using a previously described

526 pipeline (48), and analyzed with RepeatMasker (49), TransposonPSI (50), and
527 LTRharvest (51). The results were further analyzed using the
528 one_code_to_find_them_all script (52). Telomeric repeats were identified by scanning
529 for the motif (TTAGGG)n in scaffold sequences (53).
530 Genome comparison between PC9 and PC9.15 was performed using Circos (v0.69.0)
531 (54) and D-genies (Minimap v2.24) (34) to visualize synteny and structural differences.
532 Mating-type loci from both genomes were aligned using Easyfig (55) or clinker (56),
533 and protein-level comparison of HD1, HD2, Ste3, and Phb were performed with
534 needleall (57). Multiple sequence alignments of HD, Ste3, and Phb proteins were
535 generated using MEGA11 with the MUSCLE algorithm (58). A phylogenetic tree was
536 constructed by using IQ-TREE v3.0.1 (59) and further visualized using iTOL v7 (60).
537 The HD1/HD2 and receptor protein sequences used for phylogenetic tree construction
538 were obtained from *Schizophyllum commune*. The corresponding sequences were
539 retrieved from NCBI GenBank. The GenBank accession numbers can be found in S7
540 Table.
541 Multiple sequence alignments of HD1, HD2, Ste3, and Phb proteins were generated
542 with the T-coffee program (61), and alignment results were visualized with Jalview
543 v2.11.5.0 (62).

544 **Cell wall Staining and imaging**

545 The fungal cultures were stained with SCRI Renaissance 2200 (SR2200), which labels
546 fungal cell walls without affecting growth, and imaged using a LSM980 Airyscan 2
547 confocal microscope (Carl Zeiss).

548 Statistics

549 Two-tailed unpaired Student's *t*-test was performed to determine the statistical
550 difference between control and experimental samples in GraphPad Prism 9. $P < 0.05$
551 was considered significant; asterisks demonstrate statistical significance, as calculated
552 by two-tailed unpaired Student's *t*-test (*$P < 0.05$, **$P < 0.01$, ***$P < 0.001$, and ****P
553 < 0.0001).

554 Data availability

555 The genomic data has been deposited to National Center for Biotechnology Information
556 GenBank under the accession numbers JAQZRA000000000.1 (PC9.15), OR030114
557 (PC9 mitochondrial genome), JBQVBD000000000 (SS5), and JBQVBE000000000
558 (SS14). The accession numbers of BioProject: PRJNA1098946 (SS5) and
559 PRJNA1098945 (SS14). The raw Nanopore reads of *P. ostreatus* PC9.15, SS5, and
560 SS14 have been uploaded to the Sequence Read Archive (SRA) and are available under
561 the accession numbers SRR23581323, SRR28975996, and SRR28975997, respectively.

562 Acknowledgments

563 We thank the Genomic Core of Institute of Molecular Biology, Academia Sinica, for

Nanopore sequencing and the Bioinformatics Core of Institute of Molecular Biology, Academia Sinica, for genome assembly. We also thank Hillel Schwartz for comments and suggestions about this work.

Funding

This work was supported by the Max Planck Society, Academia Sinica Investigator Award AS-IA-111-L02, and the NSTC grant 110-2311-B-001-047-MY3 to Y. -P. H.

Author Contributions

Conceived and designed the experiments: Y.-Y.L. and Y.-P.H. Performed the experiments: Y.-Y.L. Analyzed the data: Y.-Y.L., G.V.-D.U., and Y.-P.H. Writing – original draft: Y.-Y.L. Writing – review & editing: G.V.-D.U., R. J.T., and Y.-P.H.

Figures and tables

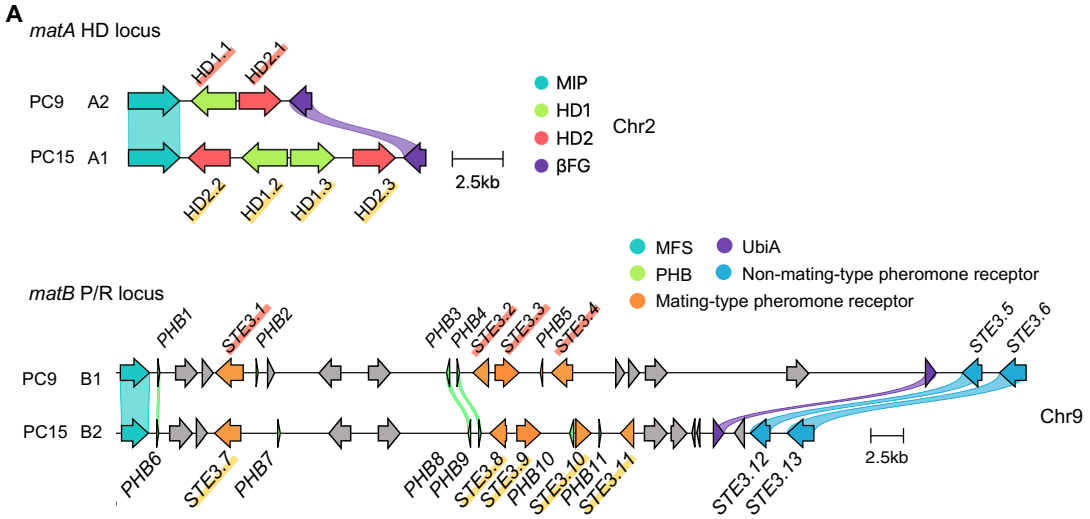

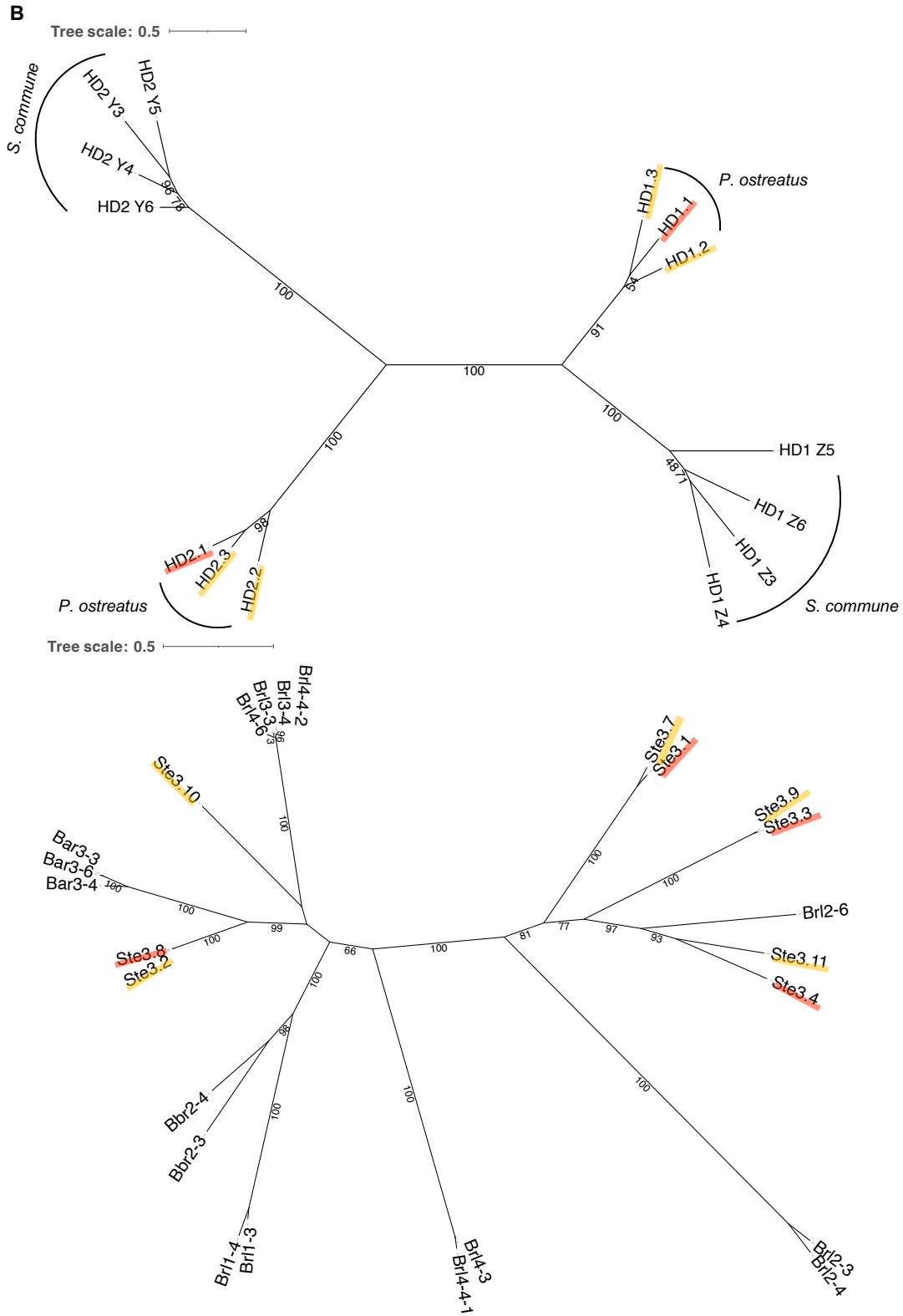
B
Tree scale: 0.5
S. commune
HD2 Y3
HD2 Y5
HD2 Y4
HD2 Y6
P. ostreatus
HD1.3
HD1.1
HD1.2
HD1 Z5
HD1 Z6
HD1 Z3
HD1 Z4
S. commune
HD2.1
HD2.3
HD2.2
P. ostreatus
Tree scale: 0.5
Brl4-4-2
Brl3-4
Brl3-3
Brl4-6
Ste3.10
Bar3-3
Bar3-6
Bar3-4
Ste3.8
Ste3.2
Ste3.7
Ste3.1
Ste3.9
Ste3.3
Brl2-6
Ste3.11
Ste3.4
Bbr2-4
Bbr2-3
Brl1-4
Brl1-3
Brl4-3
Brl4-1
Brl2-3
Brl2-4

581

582

583

584

585 **Fig 1. Characterization of mating-type loci and associated genes in *P. ostreatus*.**

586 (A) *MAT* locus alignments (amino acid-based) of strains PC9 and PC15 (clinker

587 v0.0.31). Genes encoding proteins having more than 90% identical amino acid residues

588 are linked. The color code for links and genes highlights sequence homology and grey

589 genes have no similarity to other genes in the alignment. In the *matA* locus on

590 chromosome 2 (Chr2), homeodomain genes *HD1* and *HD2* are shown in green and pink,

591 respectively; the conserved mitochondrial intermediate peptidase (*MIP*) and beta

592 flanking gene (*βFG*) are shown in teal and purple, respectively. In the *matB* locus on

593 chromosome 9 (Chr9), mating-type specific pheromone receptor genes (*STE3*) are

594 shown in orange (within *matB*) and blue (outside *matB*); pheromone genes (*PHB*) are

595 in green; the conserved MFS general substrate transporter (*MFS*) and UbiA family

596 prenyltransferase (*UbiA*) are shown in teal and purple, respectively; other genes are

597 shown in grey. Scale bars indicate 2.5 kb. (B) Phylogenetic trees of HD and Ste3

598 proteins from *P. ostreatus* (PC9 in red underline; PC15 in yellow underline) and *S.*

599 *commune* by the maximum-likelihood method using IQ-TREE.

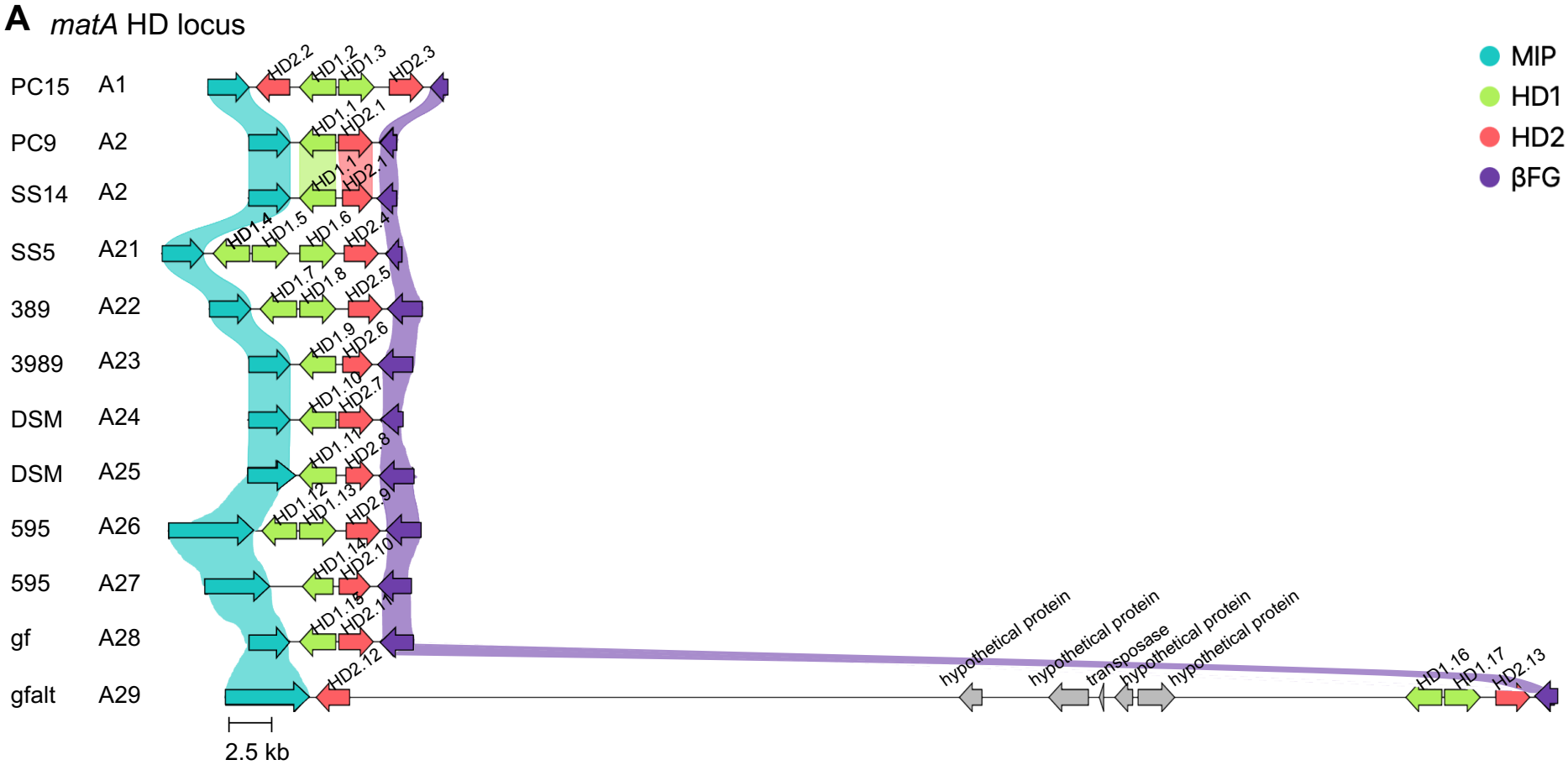
A matA HD locus
PC15 A1
PC9 A2
SS14 A2
SS5 A21
389 A22
3989 A23
DSM A24
DSM A25
595 A26
595 A27
gf A28
gfalt A29
HD2.2
HD1.2
HD1.3
HD2.3
HD1.1
HD2.1
HD1.4
HD1.5
HD1.6
HD2.4
HD1.7
HD1.8
HD2.5
HD1.9
HD2.6
HD1.10
HD2.7
HD1.11
HD2.8
HD1.12
HD1.13
HD2.9
HD1.14
HD2.10
HD1.15
HD2.11
HD2.12
hypothetical protein
hypothetical protein
transposase
hypothetical protein
hypothetical protein
HD1.16
HD1.17
HD2.13
2.5 kb
MIP
HD1
HD2
βFG

600

601

matB P/R locus

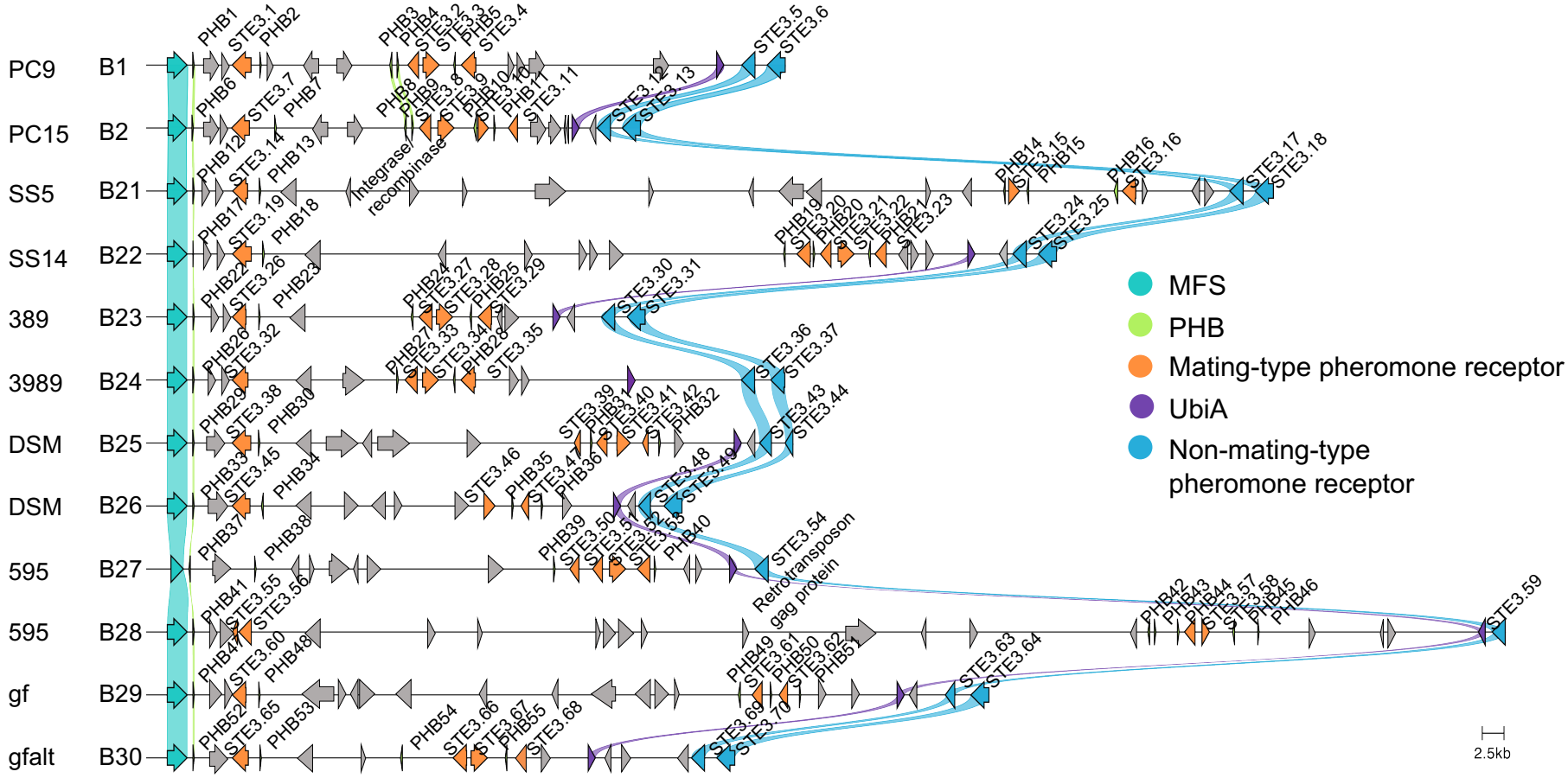

602

B

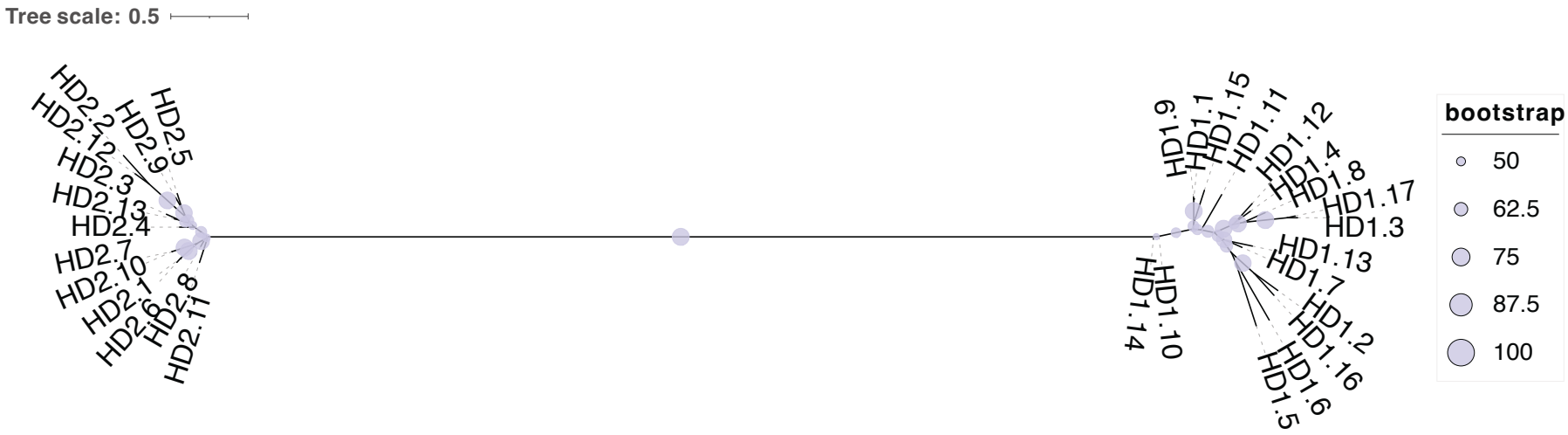
Tree scale: 0.5
HD2.2
HD2.12
HD2.3
HD2.13
HD2.4
HD2.7
HD2.10
HD2.1
HD2.6
HD2.8
HD2.11
HD2.9
HD2.5
HD1.9
HD1.1
HD1.15
HD1.11
HD1.12
HD1.4
HD1.8
HD1.17
HD1.3
HD1.13
HD1.7
HD1.2
HD1.16
HD1.6
HD1.5
HD1.10
HD1.14
bootstrap
50
62.5
75
87.5
100

603

604

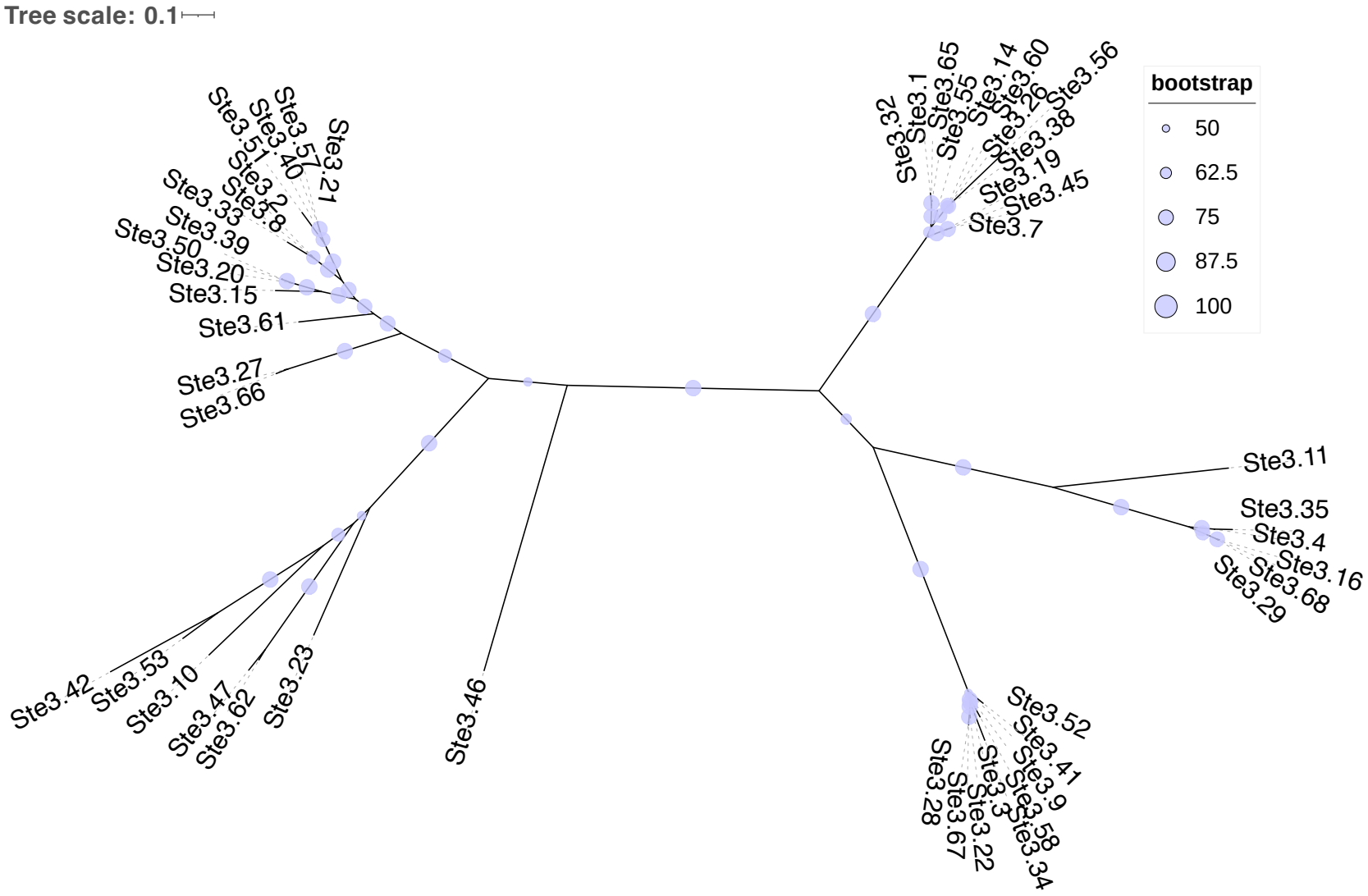
Tree scale: 0.1
bootstrap
50
62.5
75
87.5
100
Ste3.21
Ste3.57
Ste3.40
Ste3.51
Ste3.22
Ste3.8
Ste3.33
Ste3.39
Ste3.50
Ste3.20
Ste3.15
Ste3.61
Ste3.27
Ste3.66
Ste3.42
Ste3.53
Ste3.10
Ste3.47
Ste3.62
Ste3.23
Ste3.46
Ste3.32
Ste3.1
Ste3.65
Ste3.55
Ste3.14
Ste3.60
Ste3.26
Ste3.56
Ste3.38
Ste3.19
Ste3.45
Ste3.7
Ste3.11
Ste3.35
Ste3.4
Ste3.16
Ste3.68
Ste3.29
Ste3.52
Ste3.41
Ste3.9
Ste3.58
Ste3.34
Ste3.3
Ste3.22
Ste3.67
Ste3.28

605

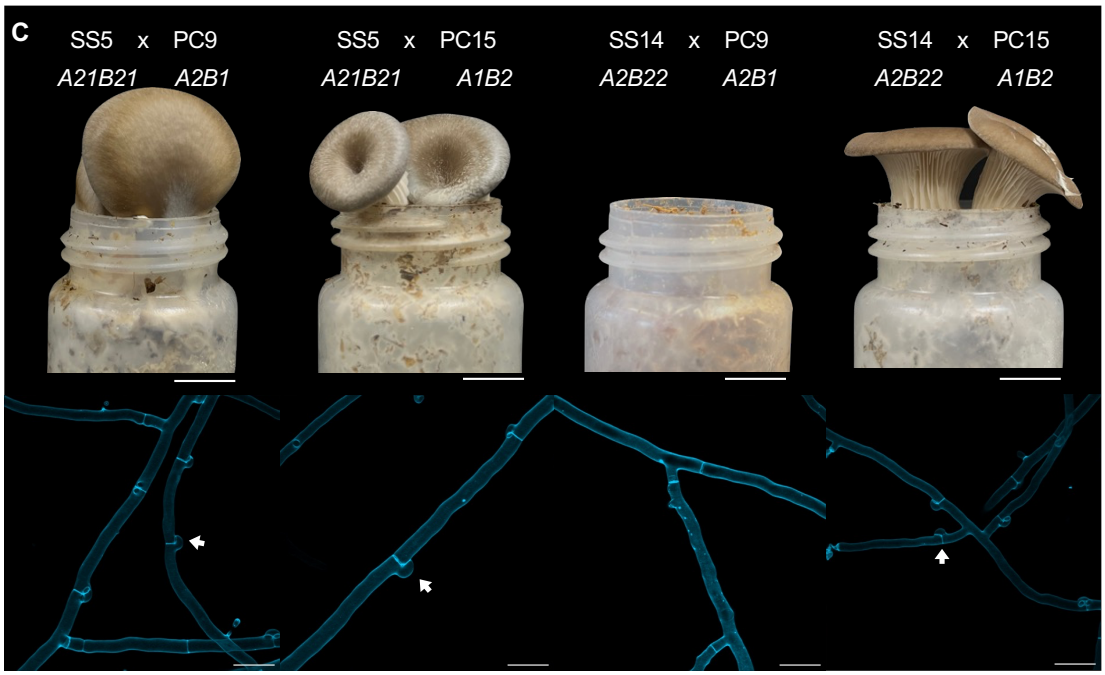

Fig 2. Comparative analysis of *matA* and *matB* loci across *P. ostreatus* strains. *MAT* locus alignments (amino acid-based) of 12 haplotypes PC9, PC15, SS5, SS14, CCMSSC00389 (389), CCMSSC03989 (3989), gfPleOstr1.1 (haplotypes gf and gfalt), and two dikaryotic strains: DSM11191 (DSM) and 595 (clinker v0.0.31). Genes encoding proteins having more than 90% identical amino acid residues are linked. The color code for links and genes highlights sequence homology and grey genes have no similarity to other genes in the alignment. Homeodomain genes *HD1* and *HD2* are shown in green and pink, respectively; the conserved *MIP* and *βFG* are shown in teal and purple, respectively. Pheromone receptor genes (*STE3*) are shown in orange (within *matB*) and blue (outside *matB*); pheromone genes (*PHB*) are in green; the conserved *MFS* and *UbiA* are shown in teal and purple, respectively; other genes are shown in grey. (B) Phylogenetic trees of 30 HD proteins and 48 Ste3 proteins from 12 *P. ostreatus*

619 haplotypes by the maximum-likelihood method using IQ-TREE. (C) Clamp connection

620 and fruiting body formation in interstrain crosses of *P. ostreatus*. Representative crosses

621 of SS5 (*A21B21*) x PC9 (*A2B1*), SS5 (*A21B21*) x PC15 (*A1B2*), SS14 (*A2B22*) x PC9

622 (*A2B1*), and SS14 (*A2B22*) x PC15 (*A1B2*) display hallmark features of successful

623 mating in a tetrapolar system, including clamp connections (arrows) and the fruiting

624 body formation. Scale bar = and 1 cm (upper panels) and 10 µm (lower panels).

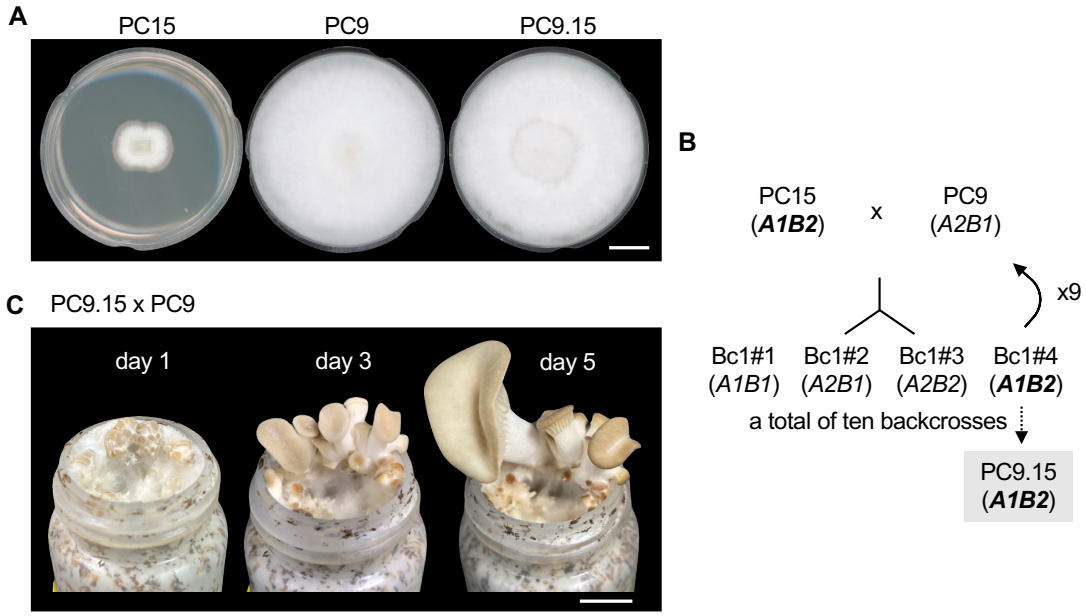

625

626 **Fig 3. Construction of the congenic strain PC9.15 with a PC9 genetic background**

627 **and PC15 mating-type loci.**

628 (A) PC9, PC15, and PC9.15 were grown on YMG agar media in 5.5-cm diameter Petri

629 plates for 10 days. Scale bar = 1 cm. (B) Crossing strategy used to generate the PC9.15

630 congenic strain: Monokaryotic "Bc1#" progeny were obtained from a PC9 x PC15 cross.

631 Progeny carrying the PC15 (*A1B2*) mating type were backcrossed to PC9 (*A2B1*) to

632 generate monokaryotic "Bc2" progeny. This process was repeated for ten crosses to

633 produce PC9.15. (C) Fruiting body development from a PC9.15 x PC9 cross at days 1,

634 3, and 5. Scale bars = 1 cm.

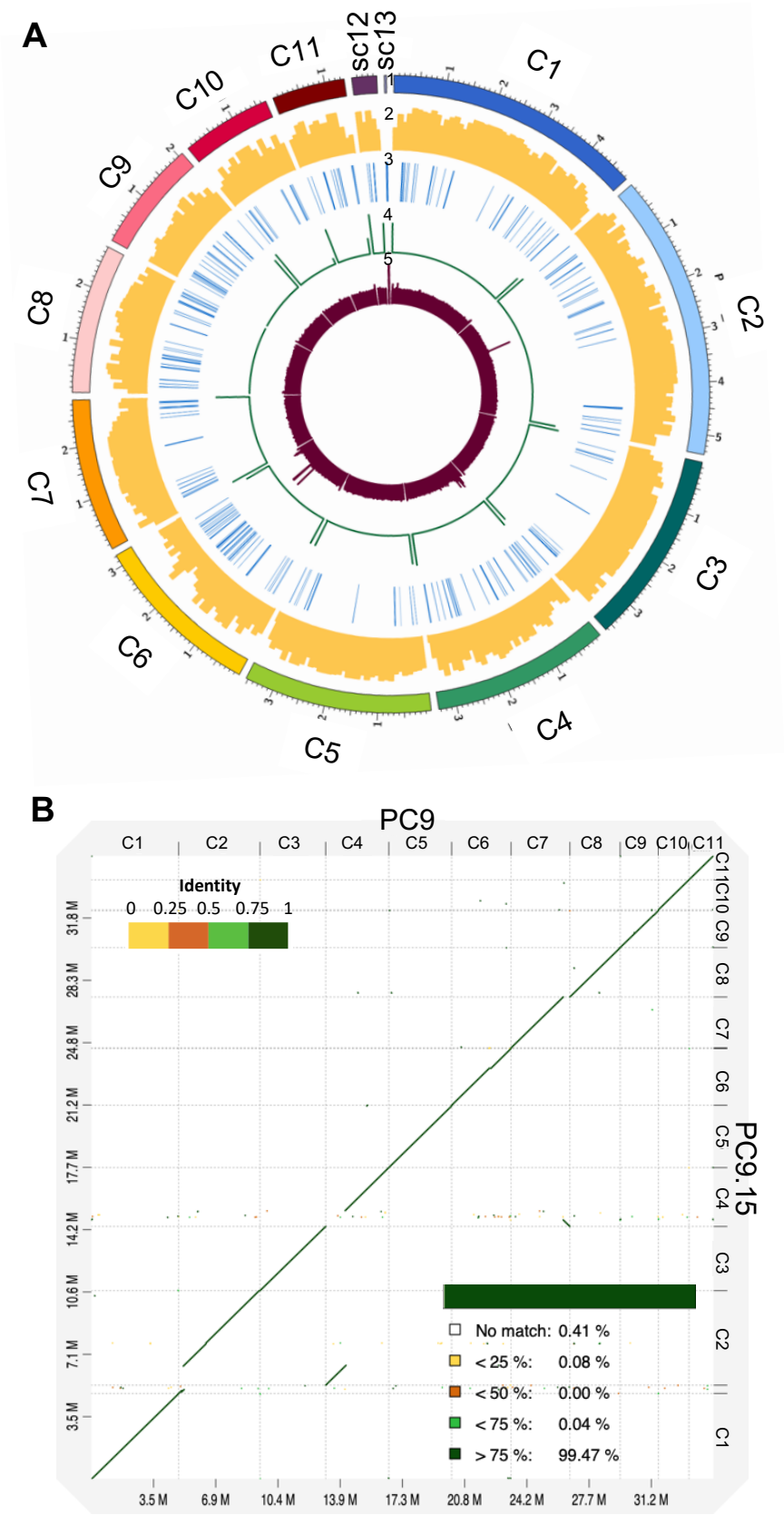
A
C1
C2
C3
C4
C5
C6
C7
C8
C9
C10
C11
sc12
sc13
B
PC9
PC9.15
Identity
0 0.25 0.5 0.75 1
No match: 0.41 %
< 25 %: 0.08 %
< 50 %: 0.00 %
< 75 %: 0.04 %
> 75 %: 99.47 %
3.5 M
6.9 M
10.4 M
13.9 M
17.3 M
20.8 M
24.2 M
27.7 M
31.2 M

635

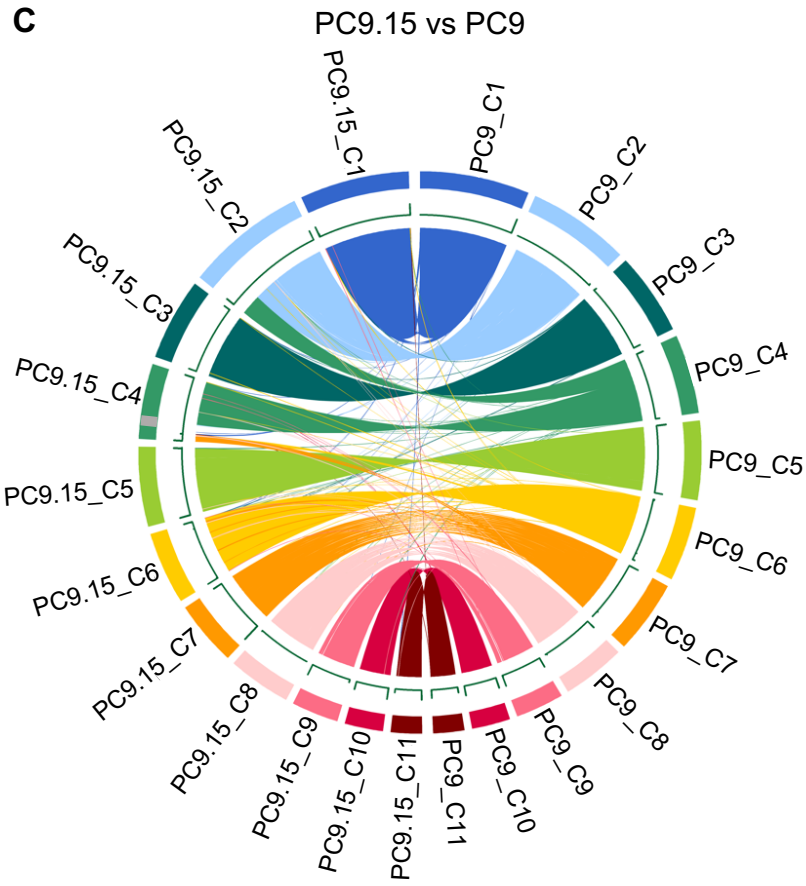
C
PC9.15 vs PC9
PC9.15_C1
PC9_C1
PC9_C2
PC9_C3
PC9_C4
PC9_C5
PC9_C6
PC9_C7
PC9_C8
PC9_C9
PC9_C10
PC9_C11
PC9.15_C11
PC9.15_C10
PC9.15_C9
PC9.15_C8
PC9.15_C7
PC9.15_C6
PC9.15_C5
PC9.15_C4
PC9.15_C3
PC9.15_C2

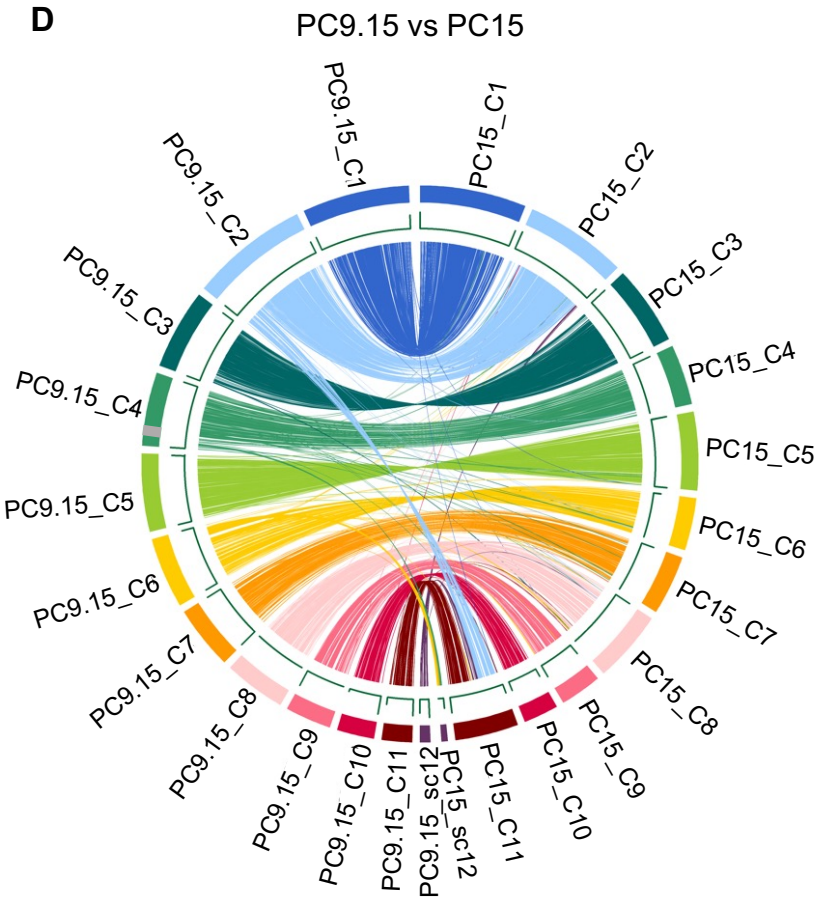
D
PC9.15 vs PC15
PC9.15_C1
PC15_C1
PC15_C2
PC15_C3
PC15_C4
PC15_C5
PC15_C6
PC15_C7
PC15_C8
PC15_C9
PC15_C10
PC15_C11
PC15_sc12
PC9.15_sc12
PC9.15_C11
PC9.15_C10
PC9.15_C9
PC9.15_C8
PC9.15_C7
PC9.15_C6
PC9.15_C5
PC9.15_C4
PC9.15_C3
PC9.15_C2

636

637 **Fig 4. Genome architecture of *P. ostreatus* congenic strain PC9.15 and comparative**

638 **analysis of assembled genomes of PC9.15, PC9, and PC15.**

639 (A) Tracks (outer to inner) represent the distribution of genomic features in our PC9.15

640 assembly: (1) size (in Mb) of PC9.15 scaffolds, with numbers prefixed by the letter "C"

641 indicating the chromosome and "sc" indicating the scaffold; (2) gene density (along

642 100-kb sliding windows, ranging between 0 and 50 protein-coding genes); (3)

643 distribution of TEs along the genome; (4) telomere repeat frequency (along 1-kb sliding

644 windows, ranging between 10 and 30 repeats); and (5) depth of sequencing coverage

645 (along 10-kb sliding windows, ranging between 0 and 150 depth). (B) Dot-plot

646 alignment of PC9.15 (query) against PC9 (reference). (C) Circos plot showing regions

647 of similarity shared by the PC9.15 (C1-C11) and PC9 (C1-C11) (identity > 95%, length

648 > 10kb). (D) Circos plot showing regions of similarity shared by the PC9.15 (C1-C12)

649 and PC15 (C1-C12) strains (identity > 95%, length > 10kb). The grey box represents

650 segment A. Tracks (outer to inner) represent the distribution of genomic features in

651 each assembly: (1) chromosome sizes (in Mb) of chromosomes, with numbers prefixed

652 by the letter "C" indicating the chromosome and "sc" indicating the scaffold; (2)

653 distribution of telomere repeats with 1-kb sliding windows, ranging between 10-30

654 repeats.

655

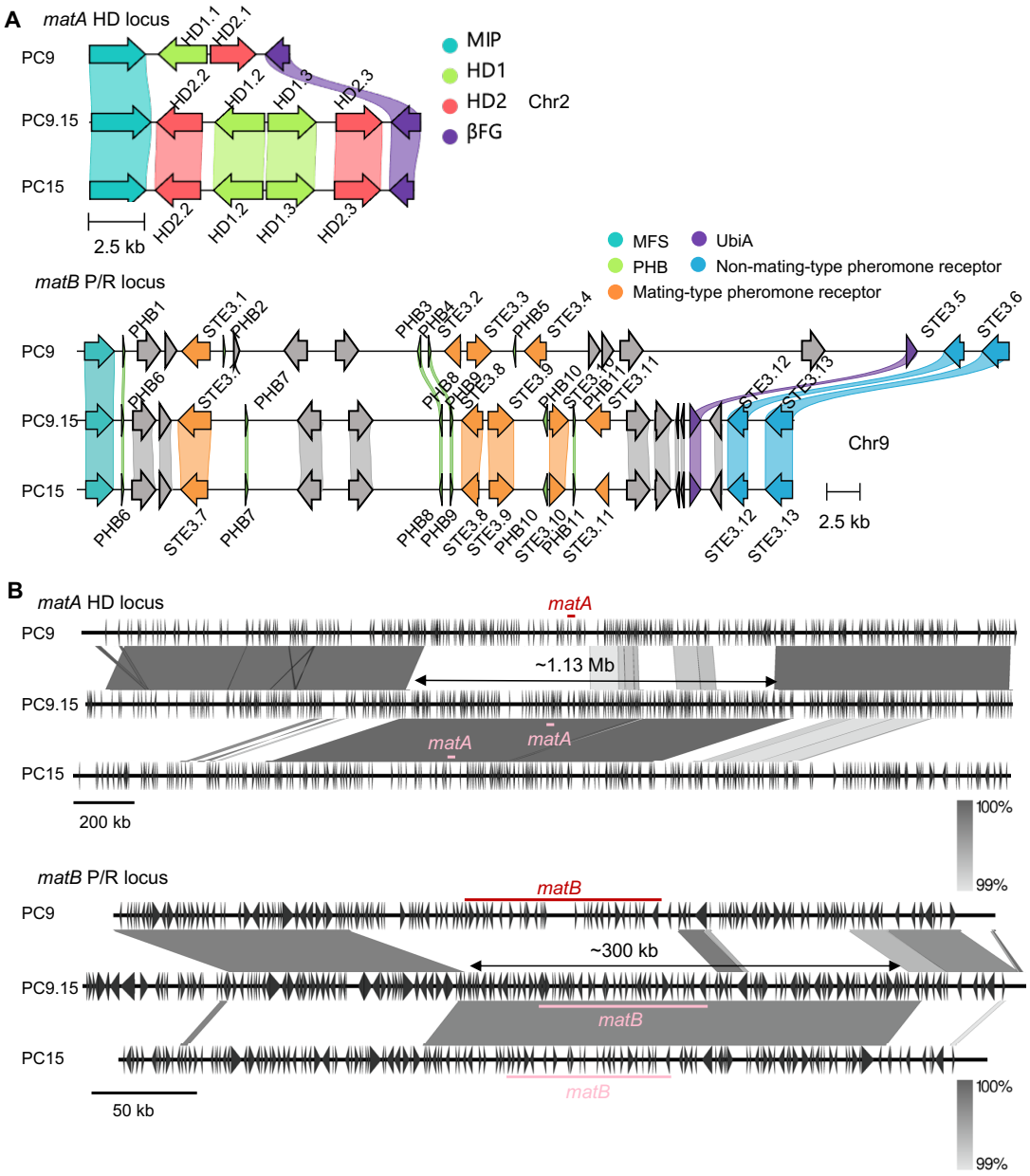

Fig 5. Characterization of mating-type loci and associated genes in PC9.15.

Structures of the *matA* and *matB* loci (A) and the large-scale chromosomal (B) *matA* and *matB* loci compared across the PC9, PC9.15, and PC15 strains.

(A) *MAT* locus alignments (amino acid-based) of strains PC9, PC9.15, and PC15 (clinker v0.0.31). Genes encoding proteins having more than 90% identical amino acid residues are linked. The color code for links and genes highlights sequence homology

663 and grey genes have no similarity to other genes in the alignment. In the *matA* locus,
664 homeodomain genes *HD1* and *HD2* are shown in green and pink, respectively; the
665 conserved *MIP* and *βFG* are shown in teal and purple, respectively. In the *matB* locus,
666 mating-type specific pheromone receptor genes (*STE3*) are shown in orange (within
667 *matB*) and blue (outside *matB*); pheromone genes (*PHB*) are in green; the conserved
668 MFS and UbiA are shown in teal and purple, respectively; other genes are shown in
669 grey. (B) Large-scale alignment of the *matA* and *matB* loci between PC9, PC9.15, and
670 PC15. The *matA* and *matB* loci of PC9 is shown as red line; those of PC9.15 and PC15
671 are shown as pink lines. The shades of grey show nucleotide sequence identity. The
672 figures were generated by Easyfig v2.2.2.
673

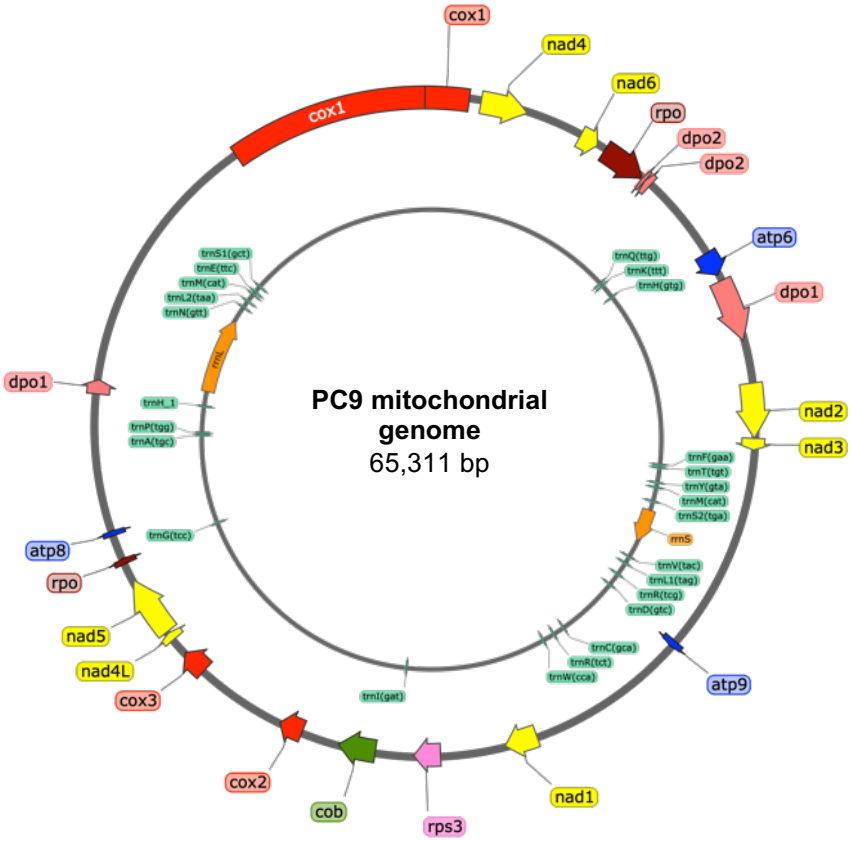

674

675 **Fig 6. Circular map of the mitochondrial genome of *P. ostreatus* PC9.** Tracks (outer

676 to inner) show: (1) annotation of mitochondrial DNA-encoded genes: subunits of

677 cytochrome c oxidase/complex IV (red), NADH dehydrogenase/complex I (yellow),

678 ATP synthase/complex V (blue), apocytochrome b *cob* (green), ribosomal small subunit

679 protein *rps3* (pink), DNA polymerase *dpo* (salmon) and DNA-directed RNA

680 polymerase *rpo* (brown); (2) annotation of RNA genes: ribosomal RNA genes *rrnS* and

681 *rrnL* (orange) and 25 transfer RNA (green).

682

683

684

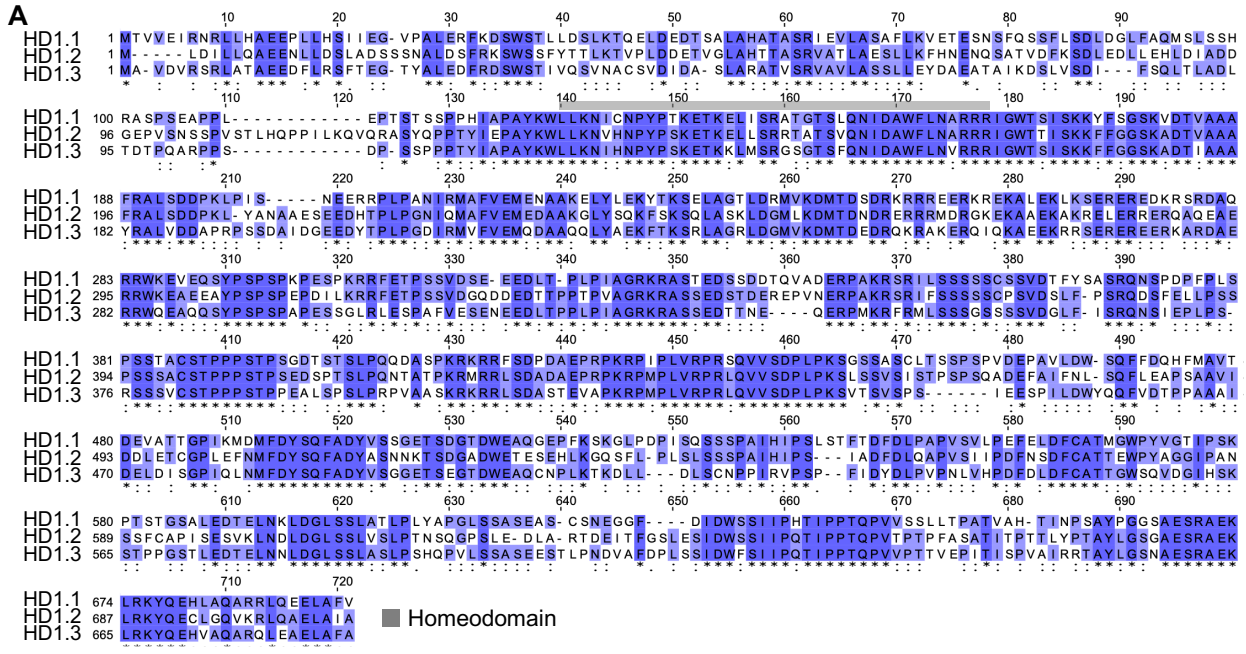

685

C

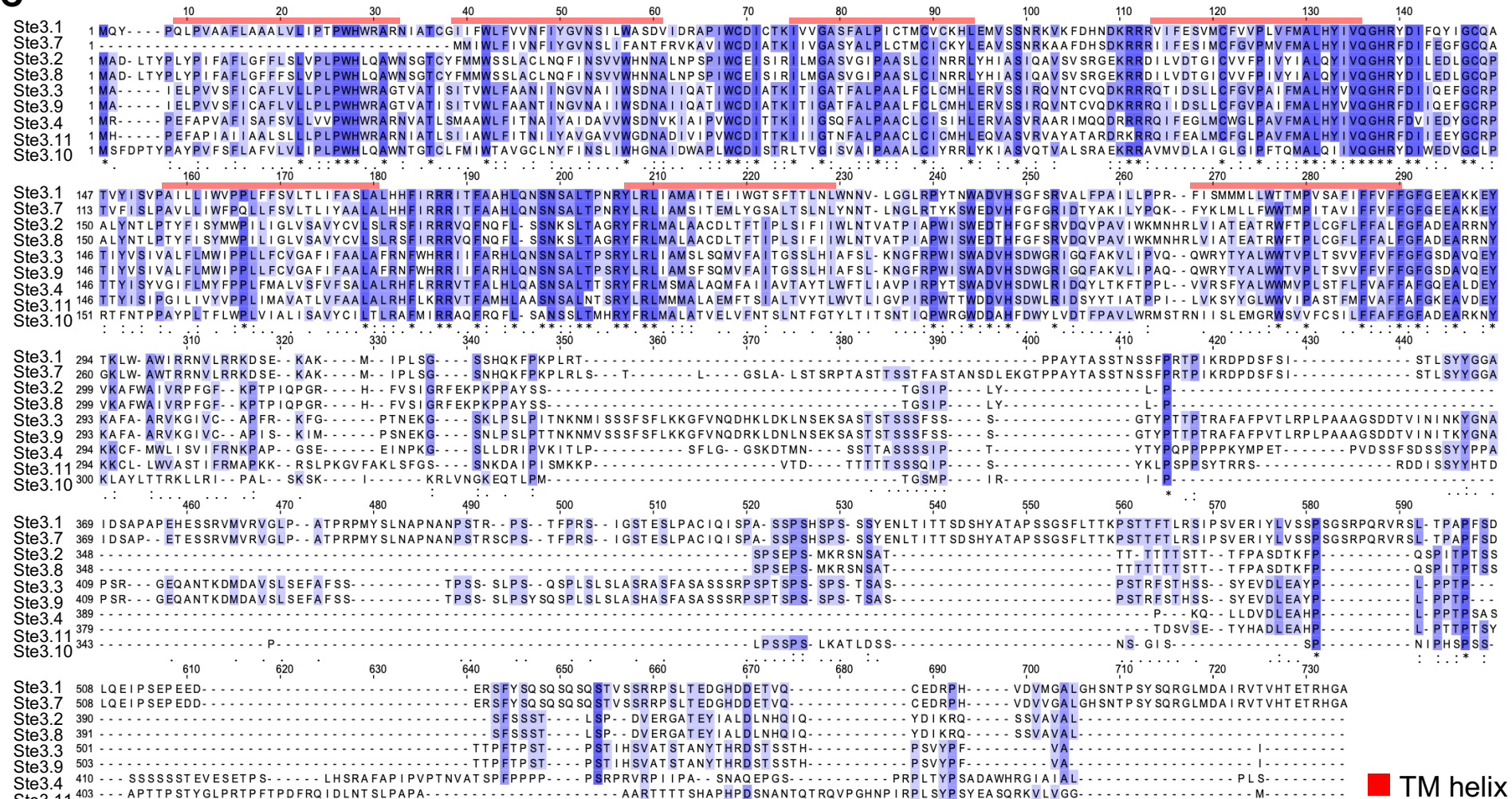
Ste3.1
Ste3.7
Ste3.2
Ste3.8
Ste3.3
Ste3.9
Ste3.4
Ste3.11
Ste3.10
TM helix

D

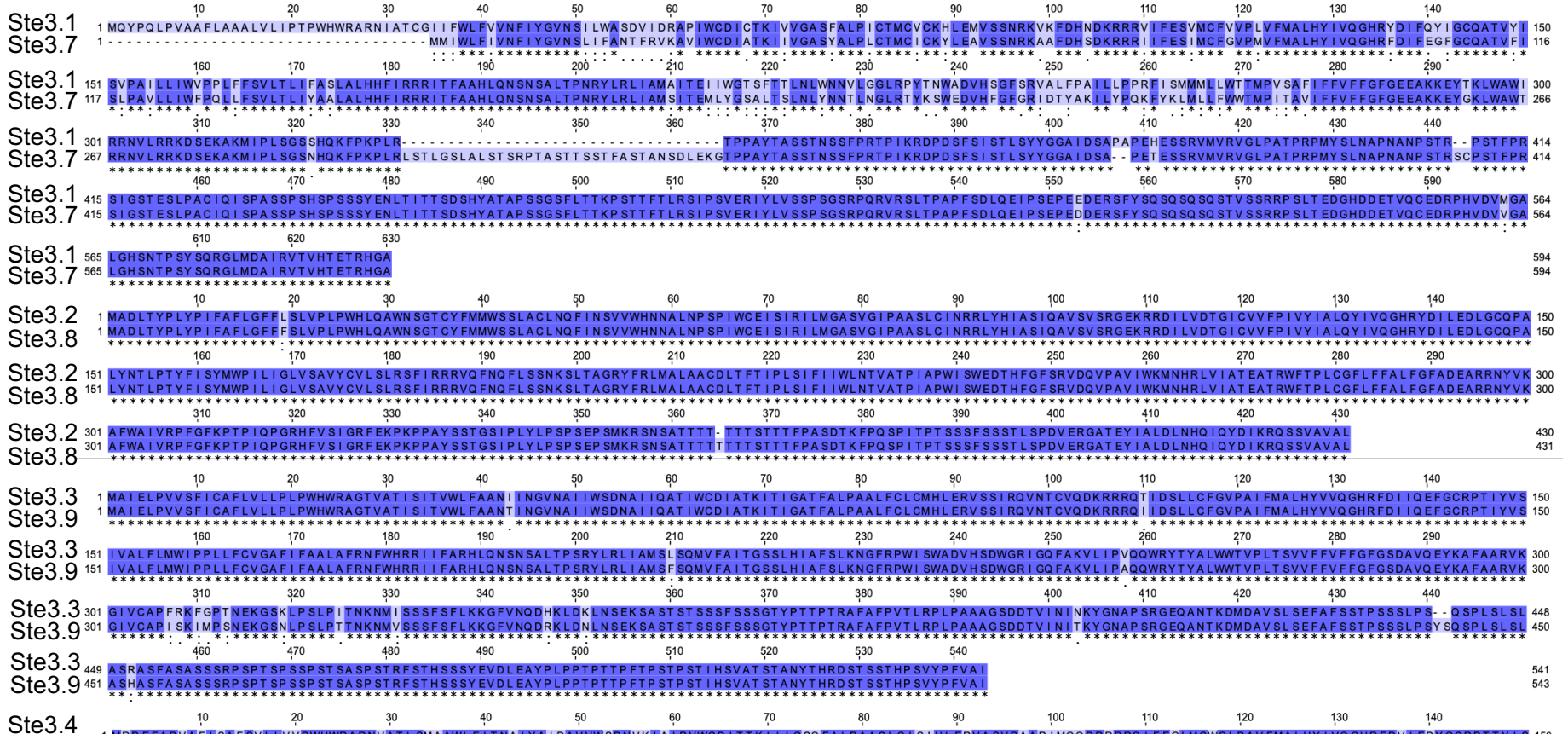

E

```
                    10        20        30        40        50        60        70
Phb1   1 MDIFFTLVAYIVPGTAQP----------------ASSSASSSSTSNDS--GPC-SDDERTRSG--AFCYCVVT 52
Phb2   1 MDAFTTSDDLATILLE----------------LEPAAAHDTSQPQDDF--GGVPLDEDHPS-Q--IITWCTIA 52
Phb3   1 MDTFNRLESLLTLSSSSWTEA--------GADTEVAPSSSSSHTTDDG-LFDLPVDAERDIPGFTSRGWCIIS 64
Phb4   1 MDFFATTTILEQLAASIPS--------LPSIPVESSSHPDSNNDEPDE--LPVPVDEERYGVGV-TNSWCTVS 62
Phb5   1 MDTFISLDELFIEGSESD-----------VDIMSQTSSD-SEDEDSDCEMPMPVNFERRGPGGAAQFWCIIS 60
Phb6   1 MDIFFTLVAYIVPGTALP----------------ASSSASSSSTSNDS--GPC-SDDERTRSG--AFCYCVVT 52
Phb7   1 MDEFHHINFDAIPSTLTPVSAIASASISSSIPTSCASSI-GSDGGDDG--LDGILDEDKPW-S--PVTWCTIA 67
Phb8   1 MDTFNRLESLLTLSSSSWTEA--------GADTEVAPS-SSSHTTDDG-LFDLPVDAERDIPGFTSRGWCIIS 63
Phb9   1 MDFFATTTILEQLAASIPS--------LPSIPVESSSHPDSNNDEADE--LPVPVDEERYGVGV-TNSWCTVS 62
Phb10  1 MDEFLTITIPEDDC-SSW----------------VLSSSS-PEDEEEQ--EQLPVDFERRAGG--ATFWCTIA 51
Phb11  1 MDSFQSFSLPVDEPASED----------------VIPISASAEQEDEL--IKQLCDADAHMP---YGGNCVIS 52
         ** * ..  .     . .                 .  .: .:   ..:    .  :.* ::   :     :*.:.
```

688

689 **S1 Fig. Protein sequence alignment of mating type-related proteins in *P. ostreatus*.**

690 Alignment of (A) HD1, (B) HD2, (C and D) Ste3, and (E) Phb proteins from strains
691 PC9 and PC15. Three levels of shading indicate degrees of sequence similarity: dark
692 blue background with an asterisk (*) indicates identical amino acids, intermediate blue
693 background with a colon (:) indicates conserved amino acids, and light blue with a dot
694 (.) indicates semi-conserved amino acids. Grey and red shading indicate the
695 homeodomain regions in HD proteins and the transmembrane (TM) helix regions in
696 Ste3 proteins, respectively.

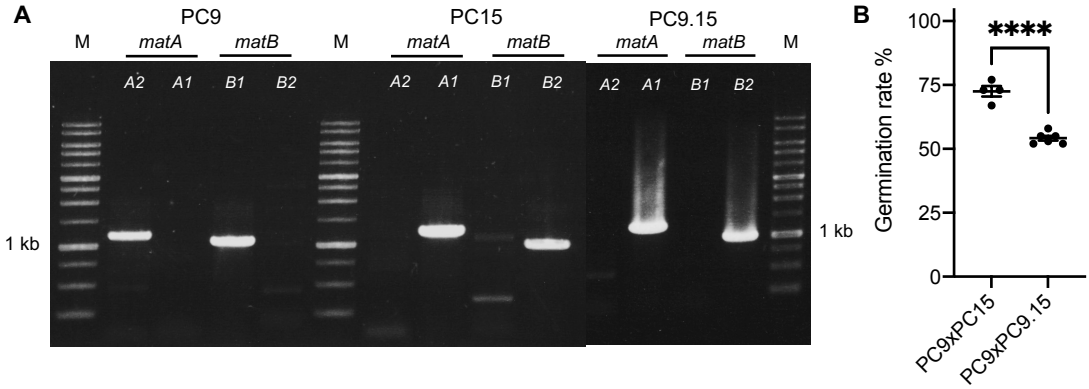

697

698 **S2 Fig. Confirmation of mating-type loci and germination rates in congenic strain**
699 **PC9.15.**

700 (A) PCR amplification of the *matA* and *matB* loci in PC9, PC15, and the congenic strain
701 PC9.15 using mating-type specific primers: PC9-*matA*-F/R, PC9-*matB*-F/R, PC15-
702 *matA*-F/R, and PC15-*matB*-F/R. (B) Germination rates of PC9 x PC15 and PC9 x
703 PC9.15. Statistical significance was calculated using a two-tailed unpaired Student's *t*-
704 test.

A

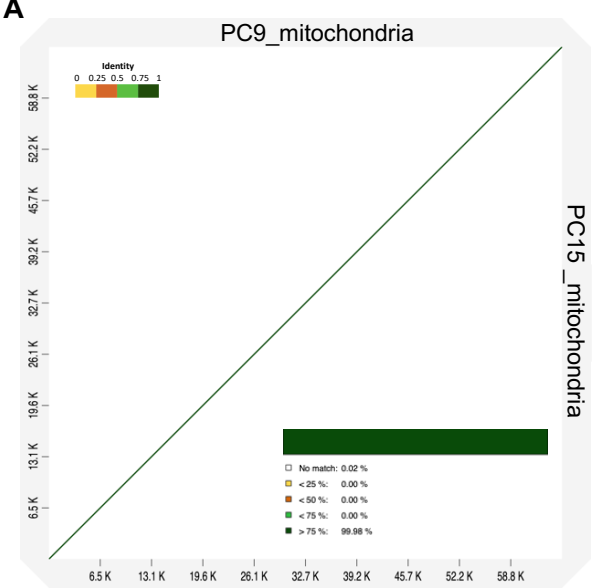
PC9_mitochondria
PC15_mitochondria
Identity
0 0.25 0.5 0.75 1
No match: 0.02 %
< 25 %: 0.00 %
< 50 %: 0.00 %
< 75 %: 0.00 %
> 75 %: 99.98 %
6.5 K 13.1 K 19.6 K 26.1 K 32.7 K 39.2 K 45.7 K 52.2 K 58.8 K

B

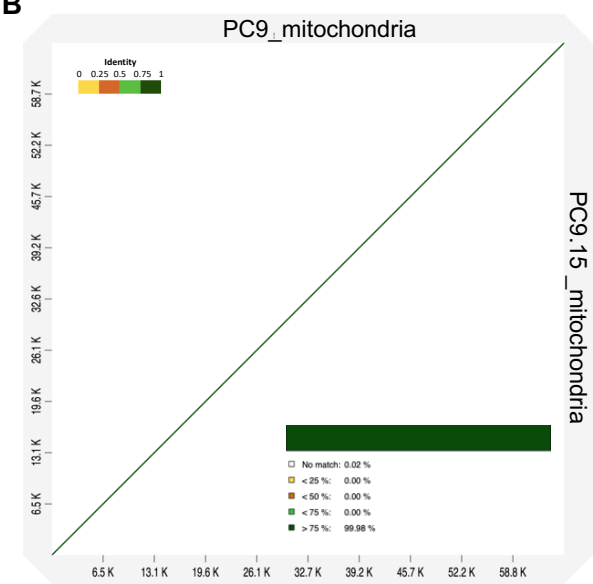
PC9_mitochondria
PC9.15_mitochondria
Identity
0 0.25 0.5 0.75 1
No match: 0.02 %
< 25 %: 0.00 %
< 50 %: 0.00 %
< 75 %: 0.00 %
> 75 %: 99.98 %
6.5 K 13.1 K 19.6 K 26.1 K 32.7 K 39.2 K 45.7 K 52.2 K 58.8 K

C

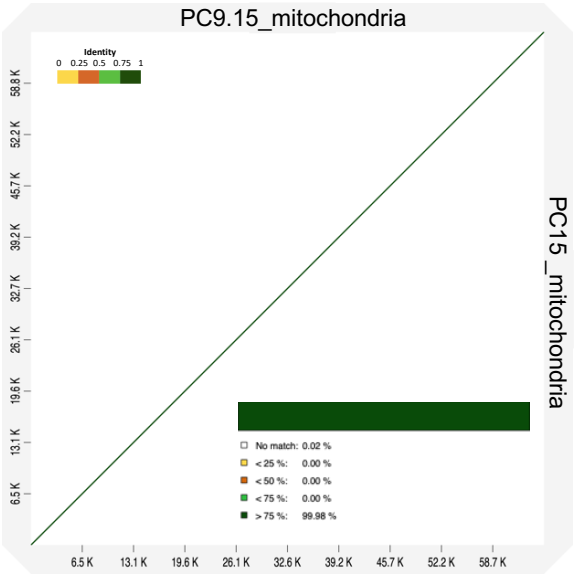
PC9.15_mitochondria
PC15_mitochondria
Identity
0 0.25 0.5 0.75 1
No match: 0.02 %
< 25 %: 0.00 %
< 50 %: 0.00 %
< 75 %: 0.00 %
> 75 %: 99.98 %
6.5 K 13.1 K 19.6 K 26.1 K 32.6 K 39.2 K 45.7 K 52.2 K 58.7 K

705

706 **S3 Fig. Comparative analysis of mitochondrial genomes of PC9, PC9.15, and PC15.**

707 Dot-plot alignment generated by D-Genies minimap v2.24 showing the mitochondrial

708 genomes of *P. ostreatus* strains: (A) PC9 (target) vs. PC15 (query), (B) PC9 (target) vs.

709 PC9.15 (query), and (C) PC9.15 (target) vs. PC15 (query).

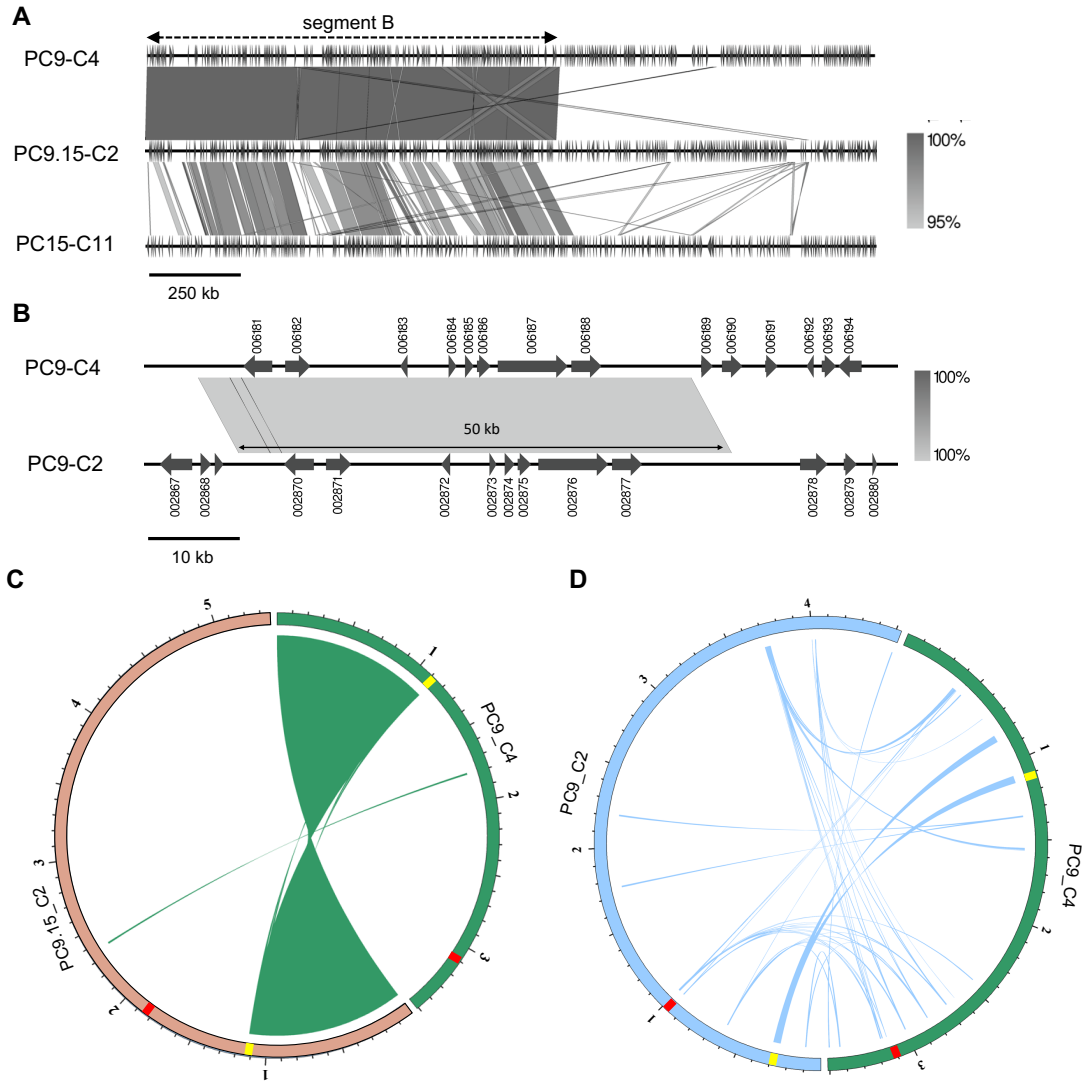

710

711 **S4 Fig. Translocation sites between the PC9 and PC9.15 genomes.**

712 (A) Partial sequence alignment of PC9 chromosome 4 (PC9_C4), PC9.15 chromosome

713 2 (PC9.15_C2), and PC15 chromosome 11 (PC15_C11). (B) Partial sequence alignment

714 of PC9 chromosome 4 (PC9_C4) and PC9 chromosome 2 (PC9_C2). (C and D) Circos

715 plots showing regions of high similarity (identity > 95%, length > 10kb) between PC9

716 chromosome 4 (PC9_C4) and PC9.15 chromosome 2 (PC9.15_C2) (C) and PC9

717 chromosome 4 (PC9_C4) and PC9 chromosome 2 (PC9_C2) (D). Red boxes represent

718 centromere region and yellow boxes represent segment B. The letter "C" indicates the

719 chromosome.

720

Reference

1. Sánchez C. Cultivation of *Pleurotus ostreatus* and other edible mushrooms. Appl Microbiol Biotechnol. 2010;85(5):1321-37.
2. Nakazawa T, Kawauchi M, Otsuka Y, Han J, Koshi D, Schiphof K, et al. *Pleurotus ostreatus* as a model mushroom in genetics, cell biology, and material sciences. Applied Microbiology and Biotechnology. 2024;108(1):217.
3. Thorn RG, Barron GL. Carnivorous mushrooms. Science. 1984;224(4644):76-8.
4. Lee C-H, Chang H-W, Yang C-T, Wali N, Shie J-J, Hsueh Y-P. Sensory cilia as the Achilles heel of nematodes when attacked by carnivorous mushrooms. Proceedings of the National Academy of Sciences. 2020;117(11):6014.
5. Lee C-H, Lee Y-Y, Chang Y-C, Pon W-L, Lee S-P, Wali N, et al. A carnivorous mushroom paralyzes and kills nematodes via a volatile ketone. Science Advances. 2023;9(3):eade4809.
6. Ni M, Feretzaki M, Sun S, Wang X, Heitman J. Sex in fungi. Annual Review of Genetics. 2011;45:405-30.
7. Lin X, Heitman J. Mechanisms of homothallism in fungi and transitions between heterothallism and homothallism. Sex in Fungi. 2007. p. 35-57.
8. Fraser JA, Heitman J. Fungal mating-type loci. Current Biology. 2003;13(20):R792-5.
9. Lee N, Bakkeren G, Wong K, Sherwood JE, Kronstad JW. The mating-type and pathogenicity locus of the fungus *Ustilago hordei* spans a 500-kb region. Proceedings of the National Academy of Sciences. 1999;96(26):15026-31.
10. Lengeler KB, Fox DS, Fraser JA, Allen A, Forrester K, Dietrich FS, et al. Mating-type locus of *Cryptococcus neoformans*: a step in the evolution of sex chromosomes. Eukaryot Cell. 2002;1(5):704-18.
11. Larraya L, Peñas MM, Pérez G, Santos C, Ritter E, Pisabarro AG, et al. Identification of incompatibility alleles and characterisation of molecular markers genetically linked to the *A* incompatibility locus in the white rot fungus *Pleurotus ostreatus*. Current Genetics. 1999;34(6):486-93.
12. Larraya LM, Pérez G, Iribarren I, Blanco JA, Alfonso M, Pisabarro AG, et al. Relationship between monokaryotic growth rate and mating type in the edible basidiomycete *Pleurotus ostreatus*. Applied and environmental microbiology. 2001;67(8):3385-90.
13. Shnyreva AV, Shnyreva AA. Structure analysis of the *matA* locus of sexual compatibility in the edible mushroom *Pleurotus ostreatus*. Doklady Biochemistry and Biophysics. 2023;511(1):203-11.
14. Larraya LM, Pérez G, Peñas MM, Baars JJP, Mikosch TSP, Pisabarro AG, et al.

758 Molecular karyotype of the white rot fungus *Pleurotus ostreatus*. Applied and
759 Environmental Microbiology. 1999;65(8):3413.
760 15. Chadwick BJ, Lin X. On the history and applications of congenic strains in
761 *Cryptococcus* research. Pathogens. 2020;9(9).
762 16. Nielsen K, Marra RE, Hagen F, Boekhout T, Mitchell TG, Cox GM, et al.
763 Interaction between genetic background and the mating-type locus in *Cryptococcus*
764 *neoformans* virulence potential. Genetics. 2005;171(3):975-83.
765 17. Lin X, Huang JC, Mitchell TG, Heitman J. Virulence attributes and hyphal
766 growth of *C. neoformans* are quantitative traits and the MATα allele enhances
767 filamentation. PLoS Genetics. 2006;2(11):e187.
768 18. Lee Y-Y, Vidal-Diez de Ulzurrun G, Schwarz EM, Stajich JE, Hsueh Y-P.
769 Genome sequence of the oyster mushroom *Pleurotus ostreatus* strain PC9. G3
770 Genes|Genomes|Genetics. 2021;11(2).
771 19. Riley R, Salamov AA, Brown DW, Nagy LG, Floudas D, Held BW, et al.
772 Extensive sampling of basidiomycete genomes demonstrates inadequacy of the white-
773 rot/brown-rot paradigm for wood decay fungi. Proceedings of the National Academy
774 of Sciences. 2014;111(27):9923.
775 20. Alfaro M, Castanera R, Lavin JL, Grigoriev IV, Oguiza JA, Ramirez L, et al.
776 Comparative and transcriptional analysis of the predicted secretome in the
777 lignocellulose-degrading basidiomycete fungus *Pleurotus ostreatus*. Environmental
778 Microbiology. 2016;18(12):4710-26.
779 21. Castanera R, López-Varas L, Borgognone A, LaButti K, Lapidus A, Schmutz J,
780 et al. Transposable elements versus the fungal genome: Impact on whole-genome
781 architecture and transcriptional profiles. PLoS Genetics. 2016;12(6):e1006108-e.
782 22. Kües U. From two to many: Multiple mating types in Basidiomycetes. Fungal
783 Biology Reviews. 2015;29(3):126-66.
784 23. Casselton Lorna A, Olesnicky Natalie S. Molecular genetics of mating
785 recognition in Basidiomycete fungi. Microbiology and Molecular Biology Reviews.
786 1998;62(1):55-70.
787 24. Caldwell GA, Naider F, Becker JM. Fungal lipopeptide mating pheromones: a
788 model system for the study of protein prenylation. Microbiol Rev. 1995;59(3):406-22.
789 25. Raper JR. Genetics of sexuality in higher fungi. New York: Ronald Press; 1966.
790 26. Qu J, Zhao M, Hsiang T, Feng X, Zhang J, Huang C. Identification and
791 characterization of small noncoding RNAs in genome sequences of the edible fungus
792 *Pleurotus ostreatus*. Biomed Res Int. 2016;2016:2503023.
793 27. Wang L, Gao W, Wu X, Zhao M, Qu J, Huang C, et al. Genome-wide
794 characterization and expression analyses of *Pleurotus ostreatus* MYB transcription
795 factors during developmental stages and under heat stress based on de novo

796 sequenced genome. Int J Mol Sci. 2018;19(7):2052.
797 28. Wright R, Woof K. The genome sequence of the oyster mushroom, *Pleurotus*
798 *ostreatus* ((Jacq.) P. Kummer, 1871). Wellcome Open Res. 2023;8:277.
799 29. Shao Q, Li X, Chen Y, Zhang Z, Cui Y, Fan H, et al. Investigations on the fusants
800 from wide cross between white-rot fungi and *Saccharomyces cerevisiae* reveal
801 unknown lignin degradation mechanism. Frontiers in Microbiology. 2022;13:935462.
802 30. Wu J, Sun W, Zheng J, Liu J, Liang X, Liu Q, et al. Chromosome-level genome
803 announcement of the monokaryotic *Pleurotus ostreatus* strain PC80. Journal of Fungi.
804 2025; 11(8).
805 31. Seidl MF, Kramer HM, Cook DE, Fiorin GL, van den Berg GCM, Faino L, et al.
806 Repetitive elements contribute to the diversity and evolution of centromeres in the
807 fungal genus *Verticillium*. mBio. 2020;11(5).
808 32. Manni M, Berkeley MR, Seppey M, Simao FA, Zdobnov EM. BUSCO Update:
809 Novel and streamlined workflows along with broader and deeper phylogenetic
810 coverage for scoring of eukaryotic, prokaryotic, and viral genomes. Molecular
811 Biology and Evolution. 2021;38(10):4647-54.
812 33. Stajich JMPJ. Funannotate v1.8.1: Eukaryotic genome annotation 2020 [
813 34. Cabanettes F, Klopp C. D-GENIES: dot plot large genomes in an interactive,
814 efficient and simple way. PeerJ. 2018;6:e4958.
815 35. Hartmann FE, Duhamel M, Carpentier F, Hood ME, Foulongne-Oriol M, Silar P,
816 et al. Recombination suppression and evolutionary strata around mating-type loci in
817 fungi: documenting patterns and understanding evolutionary and mechanistic causes.
818 New Phytol. 2021;229(5):2470-91.
819 36. Riquelme M, Challen MP, Casselton LA, Brown AJ. The origin of multiple B
820 mating specificities in *Coprinus cinereus*. Genetics. 2005;170(3):1105-19.
821 37. Kothe E. Tetrapolar fungal mating types: Sexes by the thousands. FEMS
822 Microbiology Reviews. 1996;18(1):65-87.
823 38. Hsueh YP, Heitman J. Orchestration of sexual reproduction and virulence by the
824 fungal mating-type locus. Current Opinion in Microbiology. 2008;11(6):517-24.
825 39. Coelho MA, David-Palma M, Marincowitz S, Aylward J, Pham NQ, Yurkov AM,
826 et al. The complex evolution and genomic dynamics of mating-type loci in
827 *Cryptococcus* and *Kwoniella*. PLoS Biology. 2025;23(10):e3003417.
828 40. Fraser JA, Diezmann S, Subaran RL, Allen A, Lengeler KB, Dietrich FS, et al.
829 Convergent evolution of chromosomal sex-determining regions in the animal and
830 fungal kingdoms. PLoS Biology. 2004;2(12):e384.
831 41. Gallegos A, Jacobson DJ, Raju NB, Skupski MP, Natvig DO. Suppressed
832 recombination and a pairing anomaly on the mating-type chromosome of *Neurospora*
833 *tetrasperma*. Genetics. 2000;154(2):623-33.

42. Passer AR, Coelho MA, Billmyre RB, Nowrousian M, Mittelbach M, Yurkov AM, et al. Genetic and genomic analyses reveal boundaries between species closely related to *Cryptococcus* pathogens. mBio. 2019;10(3).
43. Chen Y, Nie F, Xie S-Q, Zheng Y-F, Dai Q, Bray T, et al. Efficient assembly of nanopore reads via highly accurate and intact error correction. Nature Communications. 2021;12(1):60.
44. Basse CW. Mitochondrial inheritance in fungi. Current Opinion in Microbiology. 2010;13(6):712-9.
45. Wang Y, Zeng F, Hon CC, Zhang Y, Leung FC. The mitochondrial genome of the Basidiomycete fungus *Pleurotus ostreatus* (oyster mushroom). FEMS Microbiol Lett. 2008;280(1):34-41.
46. Bernt M, Donath A, Jühling F, Externbrink F, Florentz C, Fritzsch G, et al. MITOS: Improved de novo metazoan mitochondrial genome annotation. Molecular Phylogenetics and Evolution. 2013;69(2):313-9.
47. Simão FA, Waterhouse RM, Ioannidis P, Kriventseva EV, Zdobnov EM. BUSCO: assessing genome assembly and annotation completeness with single-copy orthologs. Bioinformatics. 2015;31(19):3210-2.
48. Coghlan A, Tsai I, Berriman M. Creation of a comprehensive repeat library for a newly sequenced parasitic worm genome. Protocol Exchange. 2018.
49. Smit A, Hubley R & Green P. *RepeatMasker Open-4.0.* 2013-2015
50. Haas BJ. TransposonPSI. 2007-2011 Available from: http://transposonpsi.sourceforge.net.
51. Ellinghaus D, Kurtz S, Willhoeft U. LTRharvest, an efficient and flexible software for de novo detection of LTR retrotransposons. BMC Bioinformatics. 2008;9:18.
52. Bailly-Bechet M, Haudry A, Lerat E. “One code to find them all”: a perl tool to conveniently parse RepeatMasker output files. Mobile DNA. 2014;5(1):13.
53. Pérez G, Pangilinan J, Pisabarro AG, Ramírez L. Telomere organization in the ligninolytic basidiomycete *Pleurotus ostreatus*. Appl Environ Microbiol. 2009;75(5):1427-36.
54. Krzywinski M, Schein J, Birol I, Connors J, Gascoyne R, Horsman D, et al. Circos: an information aesthetic for comparative genomics. Genome Research. 2009;19(9):1639-45.
55. Sullivan MJ, Petty NK, Beatson SA. Easyfig: a genome comparison visualizer. Bioinformatics. 2011;27(7):1009-10.
56. Gilchrist CLM, Chooi YH. clinker & clustermap.js: automatic generation of gene cluster comparison figures. Bioinformatics. 2021;37(16):2473-5.
57. Rice P, Longden I, Bleasby A. EMBOSS: the European Molecular Biology Open

Software Suite. Trends Genet. 2000;16(6):276-7.
58. Tamura K, Stecher G, Kumar S. MEGA11: Molecular Evolutionary Genetics Analysis Version 11. Molecular Biology and Evolution. 2021;38(7):3022-7.
59. Minh BQ, Schmidt HA, Chernomor O, Schrempf D, Woodhams MD, von Haeseler A, et al. IQ-TREE 2: new models and fficeient methods for phylogenetic inference in the genomic era. Molecular Biology and Evolution. 2020;37(5):1530-4.
60. Letunic I, Bork P. Interactive Tree of Life (iTOL) v6: recent updates to the phylogenetic tree display and annotation tool. Nucleic Acids Research. 2024;52(W1):W78-W82.
61. Taly JF, Magis C, Bussotti G, Chang JM, Di Tommaso P, Erb I, et al. Using the T-Coffee package to build multiple sequence alignments of protein, RNA, DNA sequences and 3D structures. Nature Protocols. 2011;6(11):1669-82.
62. Waterhouse AM, Procter JB, Martin DM, Clamp M, Barton GJ. Jalview Version 2—a multiple sequence alignment editor and analysis workbench. Bioinformatics. 2009;25(9):1189-91.

889 # Supporting information

890 **S1 Fig. Protein sequence alignment of mating type-related proteins in *P. ostreatus*.**

891 Alignment of (A) HD1, (B) HD2, (C and D) Ste3, and (E) Phb proteins from strains

892 PC9 and PC15. Three levels of shading indicate degrees of sequence similarity: dark

893 blue background with an asterisk (*) indicates identical amino acids, intermediate blue

894 background with a colon (:) indicates conserved amino acids, and light blue with a dot

895 (.) indicates semi-conserved amino acids. Grey and red shading indicate the

896 homeodomain regions in HD proteins and the transmembrane (TM) helix regions in

897 Ste3 proteins, respectively.

898 **S2 Fig. Confirmation of mating-type loci and germination rates in congenic strain**

899 **PC9.15.**

900 (A) PCR amplification of the *matA* and *matB* loci in PC9, PC15, and the congenic strain

901 PC9.15 using mating-type specific primers: PC9-*matA*-F/R, PC9-*matB*-F/R, PC15-

902 *matA*-F/R, and PC15-*matB*-F/R. (B) Germination rates of PC9 x PC15 and PC9 x

903 PC9.15. Statistical significance was calculated using a two-tailed unpaired Student's *t*-

904 test.

905 **S3 Fig. Comparative analysis of mitochondrial genomes of PC9, PC9.15, and PC15.**

906 Dot-plot alignment generated by D-Genies minimap v2.24 showing the mitochondrial

907 genomes of *P. ostreatus* strains: (A) PC9 (target) vs. PC15 (query), (B) PC9 (target) vs.

908 PC9.15 (query), and (C) PC9.15 (target) vs. PC15 (query).

909 **S4 Fig. Translocation sites between the PC9 and PC9.15 genomes.**

910 (A) Partial sequence alignment of PC9 chromosome 4 (PC9_C4), PC9.15 chromosome

911 2 (PC9.15_C2), and PC15 chromosome 11 (PC15_C11). (B) Partial sequence alignment

912 of PC9 chromosome 4 (PC9_C4) and PC9 chromosome 2 (PC9_C2). (C and D) Circos

913 plots showing regions of high similarity (identity > 95%, length > 10kb) between PC9

914 chromosome 4 (PC9_C4) and PC9.15 chromosome 2 (PC9.15_C2) (C) and PC9

915 chromosome 4 (PC9_C4) and PC9 chromosome 2 (PC9_C2) (D). Red boxes represent

916 centromere region and yellow boxes represent segment B. The letter "C" indicates the

917 chromosome.

918 **S1 Table. *SET3* genes and pheromone genes in PC9, PC15, and PC9.15 genomes.**

919 **S2 Table. Ste3 proteins similarity used by needleall analysis.**

920 **S3 Table. *matA* and *matB* genes in SS5, SS14, CCMSSC00389, CCMSSC03989,**

921 **gfPleOstr1.1, gfPleOstr1.1 alternate haplotype, DSM11191, and 595 genomes.**

922 **S4 Table. Primer sets for mating type detection.**

923 **S5 Table. PC9.15 genome annotation table.**

924 **S6 Table. The similarity of PC9, PC15, and PC9.15 mitochondrial genome.**

925 **S7 Table. GenBank accession numbers of HD1/HD2 and pheromone receptors**

926 **for phylogenetic analysis.**

927